Inorganic Chemistry

Article

pubs.acs.org/IC

High Proton Mobility, Solvent Induced Single Crystal to Single Crystal Structural Transformation, and Related Studies on a Family of Compounds Formed from Mn_3 Oxo-Clusters

Saurav Bhattacharya,[†] Aninda J. Bhattacharyya,[‡] and Srinivasan Natarajan*[,†]

[†]Frameworks Solids Laboratory, Solid State and Structural Chemistry Unit, and [‡]Solid State and Structural Chemistry Unit, Indian Institute of Science, Bangalore 560012, India

Supporting Information

ABSTRACT: The reaction between 4,4′-sulfonyldibenzoic acid (H_2SDBA) and manganese under mild conditions resulted in the isolation of two new three-dimensional compounds, $[Mn_4(C_{14}H_8O_6S)_4(DMA)_2]\cdot 3DMA$, **I**, and $[Mn_3(C_{14}H_8O_6S)_3(DMA)_2(MeOH)]\cdot DMA$, **IIa**. Both structures have Mn_3 trimer oxo cluster units. While the Mn_3 oxoclusters are connected through octahedral manganese forming one-dimensional Mn−O−Mn chains in **I**, the Mn_3 units are isolated in **IIa**. The SDBA units connect the Mn−O−Mn chains and the Mn_3 clusters giving rise to the three-dimensional structure. Both compounds have coordinated and free solvent molecules. In **IIa**, two different solvent molecules are coordinated, of which one solvent can be reversibly exchanged by a variety of other similar solvents via a solvent-mediated single crystal to single crystal (SCSC) transformation. The free lattice DMA solvent molecules in **I** can be exchanged by water molecules resulting in hydrophilic channels. Proton conductivity studies on **I** reveals a high proton mobility with conductivity values of ~0.87×10^{-3} Ω^{-1} cm^{-1} at 34 °C and 98% RH, which is comparable to some of the good proton conductivity values observed in inorganic coordination polymers. We have also shown structural transformation of **I** to **IIa** through a possible dissolution and recrystallization pathway. In addition, both **I** and **IIa** appear to transform to two other manganese compounds $[H_3O][Mn_3(\mu_3\text{-}OH)(C_{14}H_8O_6S)_3(H_2O)](DMF)_5$ and $[H_3O]_2[Mn_7(\mu_3\text{-}OH)_4(C_{14}H_8O_6S)_6(H_2O)_4](H_2O)_2(DMF)_8$ under suitable reaction conditions. We have partially substituted Co in place of Mn in the Mn_3 trimer clusters forming $[CoMn_2(C_{14}H_8O_6S)_3(DMA)_2\text{-}(EtOH)]\cdot DMA$, **III**, a structure that is closely related to **IIa**. All the compounds reveal antiferromagnetic behavior. On heating, the cobalt substituted phase (compound **III**) forms a $CoMn_2O_4$ spinel phase with particle sizes in the nanometer range.

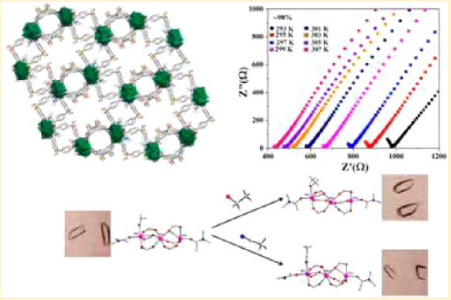

INTRODUCTION

Metal organic framework (MOF) compounds or inorganic coordination polymers (CPs) with extended three-dimensional structures have been investigated enthusiastically during the last two decades.[1] The continued interest is not only due to the fascinating and versatile structures, but also for their many properties in the areas of gas storage and separation,[2] luminescence,[3] heterogeneous catalysis,[4] magnetism,[5] drug delivery,[6] ion exchange,[7] etc. In recent years, the emphasis has also extended into investigating the possibility of hydrogen storage and proton migration in these solids.[8] Hydrogen storage and proton migration are important due to the advancements made in the fuel cell technologies where hydrogen as a fuel is an attractive option. It is well-known that the byproduct of the hydrogen fuel cell is water, making this one of the cleanest fuels.[9] Many different materials have been explored for possible proton conduction/migration with limited success. Nafion appears to be at the forefront of the fuel-cell technology.[8a,10] However, the high cost and rapid deterioration at higher temperatures are issues with Nafion prompting researchers to look for newer options.

The CP compounds with ordered pores and channels generally accommodate solvent molecules, which act as a conduit for the proton migration.[8] In addition, the carboxylate/phosphonate/sulfonate groups, present in the organic ligands, employed for the preparation of the CP frameworks, may be available as nonbonded functional groups and thus can help in the proton migration.[8] It is conceivable that the MOFs can find much use in this area as revealed by the number of studies in the recent literature.[11]

The presence of organic ligands in MOFs also provide opportunities for postsynthetic modifications.[12] There have been many studies on the use of single crystal methods to obtain possible mechanisms as well as to ascertain the nature of the modifications on a given MOF.[13] One of the commonly examined modifications is the solvent exchange/dehydration within the MOFs,[13a−g] as these studies can be investigated employing single crystal methods through single crystal−single crystal (SCSC) transformations. The structural changes that accompany such exchanges can be accommodated within the MOFs due to the flexible nature of the structures.[14]

We have been investigating inorganic coordination polymers for their interesting structures and properties. As part of the

Received: August 5, 2014
Published: February 5, 2015

DOI: 10.1021/ic5018517
Inorg. Chem. 2015, 54, 1254−1271

Table 1. Preparation Conditions Employed for the Compounds I–III

compounds	composition	initial pH	final pH	temp (°C)	time (days)	product	yield (%)[a]
I	$1MnCl_2{\cdot}4H_2O/1H_2SDBA/162DMA/124CH_3OH/1HCOOH$	~3.3	~5.4	110	3	$[Mn_4(C_{14}H_8O_6S)_4(DMA)_2]{\cdot}3DMA$	63
IIa	$1MnCl_2{\cdot}4H_2O/1H_2SDBA/216DMA/165CH_3OH/1HBF_4/1NH_4OH$	~2.1	~5.2	110	3	$[Mn_3(C_{14}H_8O_6S)_3(DMA)_2(MeOH)]{\cdot}DMA$	75
IIb	$1MnCl_2{\cdot}4H_2O/1H_2SDBA/216DMA/114CH_3CH_2OH/1HBF_4/1NH_4OH$	~2.1	~5.2	110	3	$[Mn_3(C_{14}H_8O_6S)_3(DMA)_2(EtOH)]{\cdot}DMA$	68
IIc	$1MnCl_2{\cdot}4H_2O/1H_2SDBA/216DMA/128CH_3CN/1HBF_4/1NH_4OH$	~2.1	~5.2	110	3	$[Mn_3(C_{14}H_8O_6S)_3(DMA)_2(CH_3CN)]{\cdot}DMA$	70
IId	$1MnCl_2{\cdot}4H_2O/1H_2SDBA/216DMA/370H_2O/1HBF_4/1NH_4OH$	~2.1	~5.2	110	3	$[Mn_3(C_{14}H_8O_6S)_3(DMA)_2(H_2O)]{\cdot}DMA.H_2O$	74
IIe	$1MnCl_2{\cdot}4H_2O/1H_2SDBA/216DMA/120HOCH_2CH_2OH/1HBF_4/1NH_4OH$	~2.1	~5.2	110	3	$[Mn_3(C_{14}H_8O_6S)_3(DMA)_2$(ethylene glycol)$]{\cdot}DMA$	75
III	$1CoCl_2{\cdot}4H_2O/2MnCl_2{\cdot}4H_2O/3H_2SDBA/648DMA/343CH_3CH_2OH/3HBF_4/3NH_4OH$	~2.1	~5.2	110	3	$[CoMn_2(C_{14}H_8O_6S)_3(DMA)_2(EtOH)]{\cdot}DMA$	66

[a]Yields are calculated based on the respective metals. Compositions given are molar compositions. CHN analysis for **I**: Calc (%): C 48.75; H 4.11; N 3.74; S 6.85; Found (%): C 47.88; H 4.34; N 3.93; S 6.41; for **IIa**: Calc (%): C 48.18; H 4.01; N 3.06; S 7.01; Found (%): C 47.71; H 4.21; N 3.13; S 6.83; for **IIb**: Calc (%): C 48.55; H 4.11; N 3.03; S 6.94; Found (%): C 48.13; H 4.15; N 3.15; S 7.14; for **IIc:** Calc (%): C 48.7; H 3.91; N 4.06; S 6.96; Found (%): C 47.92; H 4.12; N 4.01; S 7.03 ; for **IId:** Calc (%): C 47.16; H 3.99; N 3.05; S 6.99; Found (%): C46.27; H 4.23; N 3.33; S 6.89; for **IIe:** Calc (%): C 48.00; H 4.06; N 2.99; S 6.86; Found (%): C 48.54; H 3.99; N 3.25; S 6.97; for **III**: Calc (%): C 48.42; H 4.1; N 3.02; S 6.92; Found: C 47.49; H 3.88; N 3.35; S 6.77. Atomic absorption spectra (AAS) on the single crystals of **III** indicate a Co:Mn ratio of 1:2 (SI, Figure S1).

ongoing study on the use of 4,4′-sulfonyldibenzoic acid (H_2SDBA) as the organic ligand, we have now prepared a new family of compounds, $[Mn_4(C_{14}H_8O_6S)_4(DMA)_2]{\cdot}3DMA$, **I**, $[Mn_3(C_{14}H_8O_6S)_3(DMA)_2(X_{solvent})]{\cdot}DMA$, **IIa–IIe**, and $[CoMn_2(C_{14}H_8O_6S)_3(DMA)_2(EtOH)]{\cdot}DMA$, **III**. As part of this study, we have examined the solvent-mediated SCSC transformation, proton mobility, magnetism, and structural transformation. The use of mixed metal (Mn/Co) compound as a precursor for the synthesis of spinel oxide ($CoMn_2O_4$) nanoparticles was also investigated. In this paper we describe and discuss the findings.

EXPERIMENTAL SECTION

Synthesis of $[Mn_4(C_{14}H_8O_6S)_4(DMA)_2]{\cdot}3DMA$, I,. A solvent mixture of DMA and methanol (6 and 2 mL) was employed to dissolve $MnCl_2$ (0.4 mmol) and H_2SDBA (0.4 mmol). A total of 0.02 mL of formic acid was added to the above to reach a composition of $1MnCl_2{\cdot}4H_2O/1H_2SDBA/162DMA/124CH_3OH/1HCOOH$. The reaction mixture was heated at 110 °C for 3 days employing an indigenously fabricated 23 mL polytertafluoroethylene (PTFE) lined autoclave (stainless steel). Pale yellow block-like crystals resulted from the reaction. The products were filtered, washed (dry ethanol), and vacuum-dried (yield 63% based on Mn). A pH variation was noted during the reaction (initial = 3.3, final = 5.4). Analysis (%) for $[Mn_4(C_{14}H_8O_6S)_4(DMA)_2]{\cdot}3DMA$ [Found (calcd): C 47.88 (48.75), H 4.34 (4.11), N 3.93 (3.74), S 6.41 (6.85)].

Synthesis of $[Mn_3(C_{14}H_8O_6S)_3(DMA)_2(MeOH)]{\cdot}DMA$, IIa. A solvent mixture of DMA and methanol (6 and 2 mL) was employed to dissolve $MnCl_2{\cdot}4H_2O$ (0.3 mmol) and H_2SDBA (0.3 mmol). A total of 0.06 mL of HBF_4 and 0.023 mL of NH_4OH were added to arrive at the composition $1MnCl_2{\cdot}4H_2O/1H_2SDBA/216DMA/165CH_3OH/1HBF_4/1NH_4OH$. The reaction mixture was heated at 110 °C for 3 days in an indigenously fabricated 23 mL polytetrafluoroethylene (PTFE) lined autoclave. Pale blue block-like crystals of **IIa** resulted from this reaction. The products were filtered, washed (ethanol), and vacuum-dried (yield ~71% based on Mn). A pH variation was noted during the reaction (initial = 2.1, final = 5.2). Analysis (%) for $[Mn_3(C_{14}H_8O_6S)_3(DMA)_2(MeOH)]{\cdot}DMA$: Found (calcd): C 47.71 (48.18), H 4.21 (4.01), N 3.13 (3.06), S 6.83 (7.01)].

Solvent-Mediated Transformation Studies. Solvent-mediated exchange of the coordinated solvent molecules was attempted in a SCSC fashion of the compound **IIa**. This gave a series of compounds with the general formula $[Mn_3(C_{14}H_8O_6S)_3(DMA)_2(X_{solvent})]{\cdot}DMA$, **IIb–IIe** {where $X_{solvent}$ = ethanol in **IIb**, acetonitrile in **IIc**, water in **IId**, and ethylene glycol in **IIe**}: The studies were carried out by immersing a few single crystals of compounds **IIa** in separate glass vials containing 3 mL of DMA and 1 mL of $X_{solvent}$. The vials were capped and kept standing at room temperature for 7–8 days. The solvent exchanged crystals were collected, washed with chloroform, and dried in vacuum and examined using single crystal X-ray diffraction studies.

Bulk Synthesis of IIb–IIe and III. After the successful solvent-mediated exchange of the bound solvent molecules, we attempted to prepare the compounds in bulk employing an identical synthesis procedure, the only difference being the use of different solvent molecules. The synthesis compositions and conditions are listed in Table 1. In addition, we also attempted to partially substitute the manganese in the structure with cobalt. The heterometal compound $[CoMn_2(C_{14}H_8O_6S)_3(DMA)_2(EtOH)]{\cdot}DMA$, **III**, was also synthesized using reaction conditions that are similar to those employed for the preparation of the other compounds (Table 1). Our earlier studies in this direction were successful.[15] The heterometal compounds could be useful precursors for the preparation of some of the well-known mixed metal ceramic oxides at low temperatures as well as with small particle sizes.

INITIAL CHARACTERIZATIONS

The prepared samples were characterized initially by a plethora of techniques such as elemental analysis (C, H, N, S; Thermo Finnigan EA Flash 1112; Table 1), atomic absorption spectroscopy (AAS; PerkinElmer Analyst 200; Supporting Information (SI), Figure S1), powder X-ray diffraction (PXRD; Philips X'pert Pro; SI, Figure S2), IR (Perking-Elmer Spectrum 1000; SI, Figure S3), UV–visible spectroscopic studies (PerkinElmer Lambda 35; SI, Figure S4), photoluminescence (PerkinElmer LS-55; SI, Figure S5) and thermogravimetric analysis (TGA; Mettler-Toledo; SI, Figure S10). Mercury software (version 1.4.1) was employed to generate the simulated powder X-ray diffraction patterns from the structures determined using the single crystal XRD studies. The experimental PXRD patterns and the simulated PXRD patterns matched well for all the compounds, suggesting phase purity (SI, Figure S2). The room temperature IR spectra exhibited sharp characteristic bands (SI, Table S1, Figure S3). The various observed bands can be identified with the functional groups. Thus, the bands at ~3600–3400 cm^{-1} can

DOI: 10.1021/ic5018517
Inorg. Chem. 2015, 54, 1254–1271

Table 2. Structural Data and Refinement Parameters for Compounds I–III

	I	IIa	IIb	IIc	IId
empirical formula[a]	$C_{64}H_{32}N_2O_{26}S_4Mn_4$ ($C_{76}H_{77}N_5O_{29}S_4Mn_4$)	$C_{55}H_{55}N_3O_{22}S_3Mn_3$	$C_{60}H_{47}N_3O_{22}S_3Mn_3$ ($C_{56}H_{57}N_3O_{22}S_3Mn_3$)	$C_{56}H_{54}N_4O_{21}S_3Mn_3$	$C_{54}H_{44}N_3O_{23}S_3Mn_3$ ($C_{54}H_{55}N_3O_{23}S_3Mn_3$)
formula weight[a]	1592.92 (1872.32)	1371.02	1423.01 (1385.07)	1380.03	1363.92 (1375.03)
crystal system	triclinic	monoclinic	monoclinic	monoclinic	monoclinic
space group	$P\bar{1}$ (No. 2)	$P2_1/n$ (No. 14)	$P2_1/n$ (No. 14)	$P2_1/n$ (No. 14)	$P2_1/n$ (No. 14)
a (Å)	11.6384(18)	16.7094(3)	16.7094(3)	16.7094(3)	16.7094(3)
b (Å)	21.052(4)	20.2857(4)	20.2857(4)	20.2857(4)	20.2857(4)
c (Å)	24.247(4)	17.1936(3)	17.1936(3)	17.1936(3)	17.1936(3)
α (deg)	114.959(8)	90	90	90	90
β (deg)	102.950(9)	99.178(2)	99.178(2)	99.178(2)	99.178(2)
γ (deg)	92.406(9)	90	90	90	90
volume (Å^3)	5186.0(14)	5753.36(18)	5753.36(18)	5753.36(18)	5753.36(18)
Z	2	4	4	4	4
temperature (K)	120	120	120	120	120
ρ_{calcd} (g cm^{-3})	1.020	1.583	1.643	1.593	1.575
μ (mm^{-1})	0.611	0.841	0.845	0.841	0.842
wavelength (Å)	0.71073	0.71073	0.71073	0.71073	0.71073
θ range (deg)	1.08–26.00	2.60–26.00	2.47–26.00	2.40–26.00	2.47–26.00
R index[b] [$I > 2\sigma(I)$]	$R_1 = 0.0761$, $wR_2 = 0.2085$	$R_1 = 0.0513$, $wR_2 = 0.1362$	$R_1 = 0.0678$, $wR_2 = 0.1810$	$R_1 = 0.0621$, $wR_2 = 0.1762$	$R_1 = 0.0725$, $wR_2 = 0.2028$
R (all data)[b]	$R_1 = 0.1280$, $wR_2 = 0.2283$	$R_1 = 0.0613$, $wR_2 = 0.1434$	$R_1 = 0.0869$, $wR_2 = 0.1942$	$R_1 = 0.0766$, $wR_2 = 0.1880$	$R_1 = 0.0985$, $wR_2 = 0.2256$

	IIe	III
empirical formula[a]	$C_{60}H_{46}N_3O_{23}S_3Mn_3$ ($C_{56}H_{57}N_3O_{23}S_3Mn_3$)	$C_{60}H_{38}N_3O_{22}S_3CoMn_2$ ($C_{56}H_{57}N_3O_{22}S_3CoMn_2$)
formula weight[a]	1438.00 (1401.07)	1417.92 (1389.07)
crystal system	monoclinic	monoclinic
space group	$P2_1/n$ (No. 14)	$P2_1/n$ (No. 14)
a (Å)	16.7094(3)	16.7094(3)
b (Å)	20.2857(4)	20.2857(4)
c (Å)	17.1936(3)	17.1936(3)
α (deg)	90	90
β (deg)	99.178(2)	99.178(2)
γ (deg)	90	90
volume (Å^3)	5753.36(18)	5753.36(18)
Z	4	4
temperature (K)	120	120
ρ_{calcd} (g cm^{-3})	1.660	1.637
μ (mm^{-1})	0.847	0.913
wavelength (Å)	0.71073	0.71073
θ range (deg)	2.40–26.00	2.55–26.00
R index[b] [$I > 2\sigma(I)$]	$R_1 = 0.0729$, $wR_2 = 0.1940$	$R_1 = 0.0792$, $wR_2 = 0.2241$
R^b (all data)	$R_1 = 0.0912$, $wR_2 = 0.2073$	$R_1 = 0.0925$, $wR_2 = 0.2346$

[a]Values in brackets are the actual molecular formulas and weights, respectively accounting for the excess C and unidentified H atoms. [b]$R_1 = \Sigma||F_o| - |F_c||/\Sigma|F_o|$; $wR_2 = \{\Sigma[w(F_o^2 - F_c^2)]/\Sigma[w(F_o^2)^2]\}^{1/2}$. $w = 1/[\rho^2(F_o)^2 + (aP)^2 + bP]$. $P = [\max(F_o, O) + 2(F_c)^2]/3$, where $a = 0.1211$ and $b = 0.0000$ for **I**, $a = 0.0705$ and $b = 9.2129$ for **IIa**, $a = 0.0935$ and $b = 16.5248$ for **IIb**, $a = 0.0999$ and $b = 10.7947$ for **IIc**, $a = 0.1267$ and $b = 4.1766$ for **IId**, $a = 0.1014$ and $b = 17.4810$ for **IIe**, $a = 0.1313$ and $b = 25.8260$ for **III**.

be identified with the O–H stretching of methanol (**IIa**), ethanol (**IIb**, **III**), water (**IId**), and ethylene glycol (**IIe**).[16] In addition, the aromatic C–H stretching ($SDBA^{2-}$ ions), the asymmetric and symmetric C – H stretching of the methyl groups of the DMA, the C≡N stretching of the acetonitrile group, the asymmetric and symmetric stretching of S=O groups and the stretching frequency of C–S bond could all be identified from the IR spectroscopic studies (SI, Table S1, Figure S3).

The diffuse reflectance UV–vis spectra was recorded at room temperature for the sodium salt of the acid (Na_2SDBA) along with the compounds **I**–**III**, (SI, Figure S4). UV–vis spectroscopic studies on Na_2SDBA exhibited two absorption bands at ~218 and 287 nm, which may be due to the $\pi \rightarrow \pi^*$ and $n \rightarrow \pi^*$ transitions, respectively. The absorption bands at ~220 nm and at ~290 nm for all the compounds correspond to the $\pi \rightarrow \pi^*$ and $n \rightarrow \pi^*$ transitions, respectively, of the $SDBA^2$ anions. Absorption bands at ~250 nm, ~290 nm, ~320 nm, ~380 nm, and ~530 nm for compounds **I** and **II** correspond to the transitions from the ground state $^6A_{1g}$ of the octahedral Mn^{2+} ions to the excited states $^4A_{2g}(F)$, $^4T_{1g}(P)$, $^4T_{2g}(D)$, $^4A_{1g}$, and $^4T_{2g}$, respectively. Similar transitions have been observed previously.[17] The bands observed at ~290 nm could be the superposition of the $^6A_{1g}$ to $^4T_{1g}(P)$ transitions along with the $n \rightarrow \pi^*$ transition of the $SDBA^{2-}$. The two weak bands at ~580 nm and ~630 nm may be due to the ligand to metal charge transfer bands. For the mixed metal compound **III**, additional bands at ~565 nm and at ~612 nm were observed, which

DOI: 10.1021/ic5018517
Inorg. Chem. 2015, 54, 1254–1271

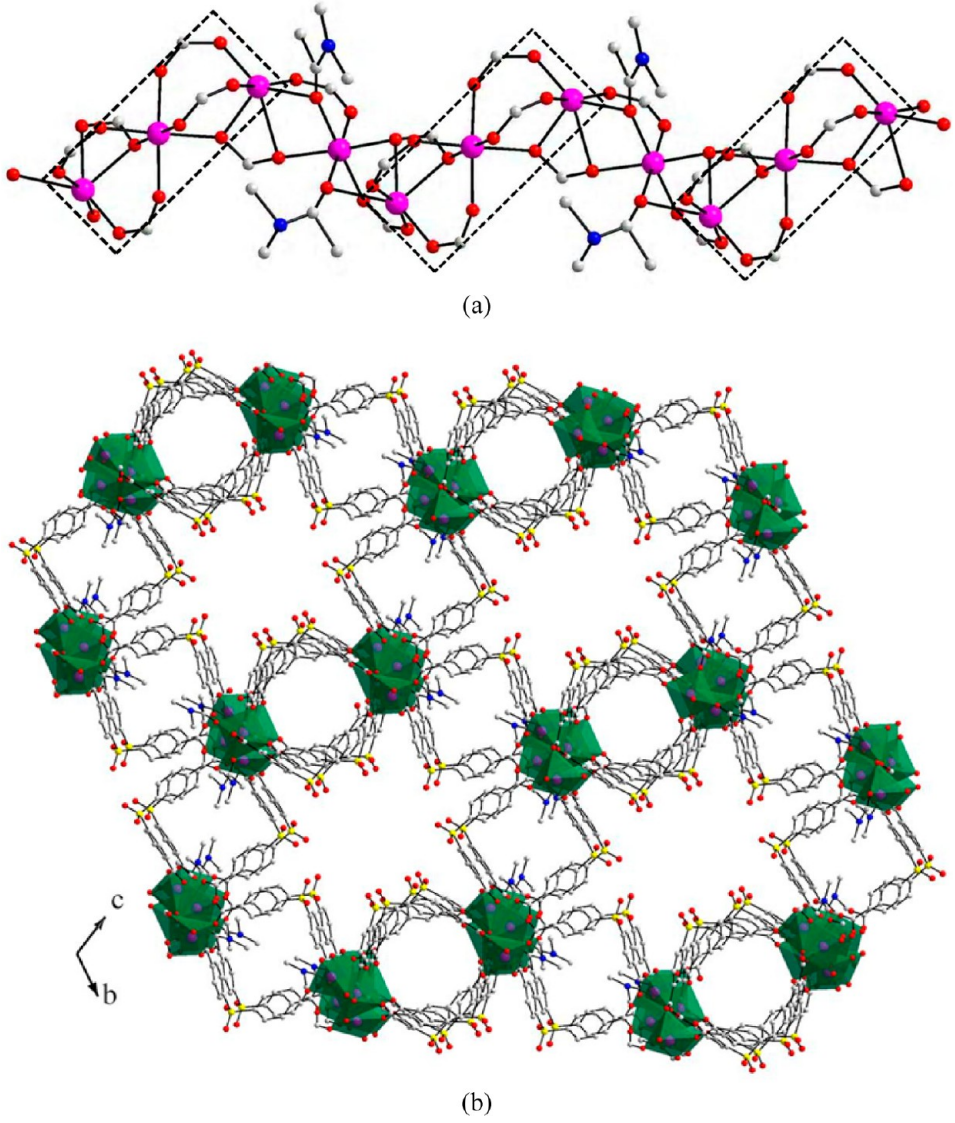

Figure 1. (a) Structure of the one-dimensional chain in **I**. The dotted rectangles show the Mn_3 trimer units. (b)The three-dimensional structure of **I**. Note that the sulfonyl groups of the $SDBA^{2-}$ anions point toward the channel.

correspond to the $^4T_1(P) \leftarrow {}^4A_2$ and the $^4T_{1g}(F) \leftarrow {}^4A_2$ transitions of the tetrahedral Co^{2+} ions, respectively.[17] The band gap in compounds **I** and **II** were found to be ∼2.85 eV and ∼3.18 eV, respectively.

Room temperature solid state photoluminescence studies were carried out on powdered samples of Na_2SDBA along with compounds **I**−**III** (SI, Figure S5). Na_2SDBA and the compounds **I**−**III** were excited using a wavelength of 250 nm. Strong emissions at ∼390 nm along with a shoulder at ∼410 nm correspond to the $\pi^* \rightarrow \pi$ and $\pi^* \rightarrow$ n transitions, respectively. The photoluminescence spectra of compounds **I**−**III** also reveal strong emissions at ∼400 nm and ∼420 nm, which can be due to the $\pi^* \rightarrow \pi$ and $\pi^* \rightarrow$ n transitions of $SDBA^{2-}$ species, respectively.[18]

STRUCTURE DETERMINATION

The structure of the compounds (**I**−**III**) were determined using single crystal X-ray diffraction.. The data sets were collected at low temperature [120(2) K] using an Oxford Xcalibur (Mova) Diffractometer equipped with an EOS detector. For collecting the single crystal diffraction data, the X-rays were generated by operating the generator at 50 kV and 0.8 mA with Mo Kα (λ = 0.710 73 Å). The cell refinements and the data reductions were performed using the program *Crysalis Red*.[19] Direct methods were employed for the structure solution, and the refinement was performed using WINGX (version 1.63.04a).[20] The lattice DMA molecules in **I** could be located from the difference Fourier maps, and the two coordinated DMA molecules could be identified. A combination of elemental analysis, IR, and TGA studies was employed to arrive at the total number of the DMA molecules. In compounds **II** and **III**, the hydrogen positions could be located on the solvent molecules (methanol, ethanol, acetonitrile, water, and ethylene glycol). The hydrogen positions, however, could not be located for the lattice water molecules in compound **IId** and for some of the DMA molecules present in the compounds **I**, **IIb**, **IId**, **IIe**, and **III**, mainly due to the atoms being disordered. One of the coordinated DMA molecules in each of the compounds **IIb**, **IIe**, **III** show 2-fold positional disorder as well as thermal disorder due to which DFIX and DANG commands were used to optimize the geometry of the DMA molecules. Final refinements were carried out using

DOI: 10.1021/ic5018517
Inorg. Chem. 2015, 54, 1254−1271

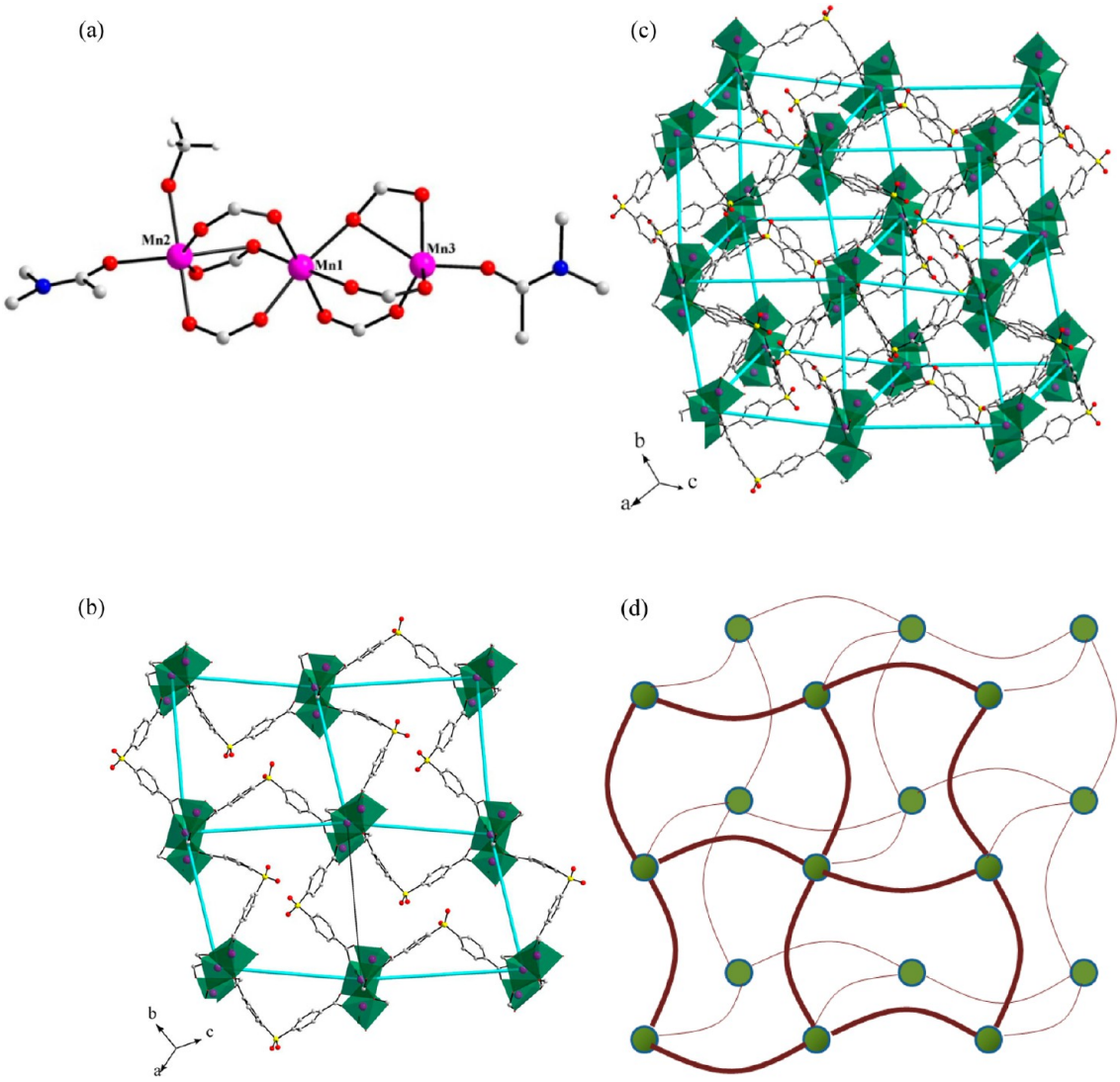

Figure 2. (a) The trinuclear cluster observed in compound **IIa**. Similar trinuclear clusters are observed in **IIb**–**IIe**. (b) View of the 2D arrangement in **II**. (c) The observed 3D structure of **II**. The *pcu* (primitive cubic) arrangement is outlined in blue. (d) A schematic of the structure of **II** (the trimer units are represented as balls and the $SDBA^{2-}$ units represented as curved lines).

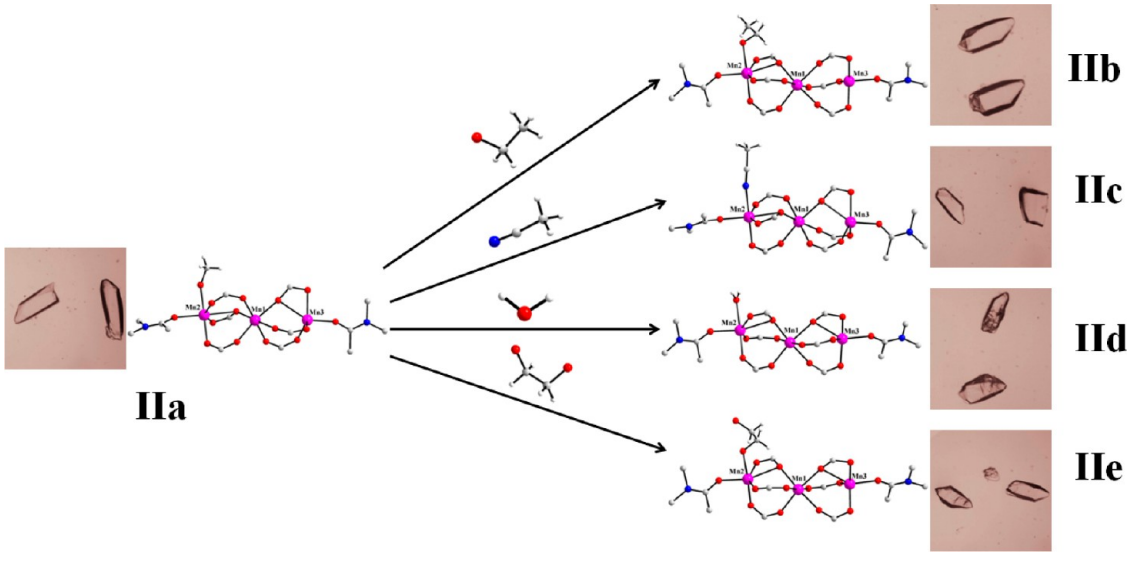

Figure 3. Pictorial representation of the trimer units of the compounds **IIa** → **IIe** under solvent-mediated SCSC transformation.

DOI: 10.1021/ic5018517
Inorg. Chem. 2015, 54, 1254–1271

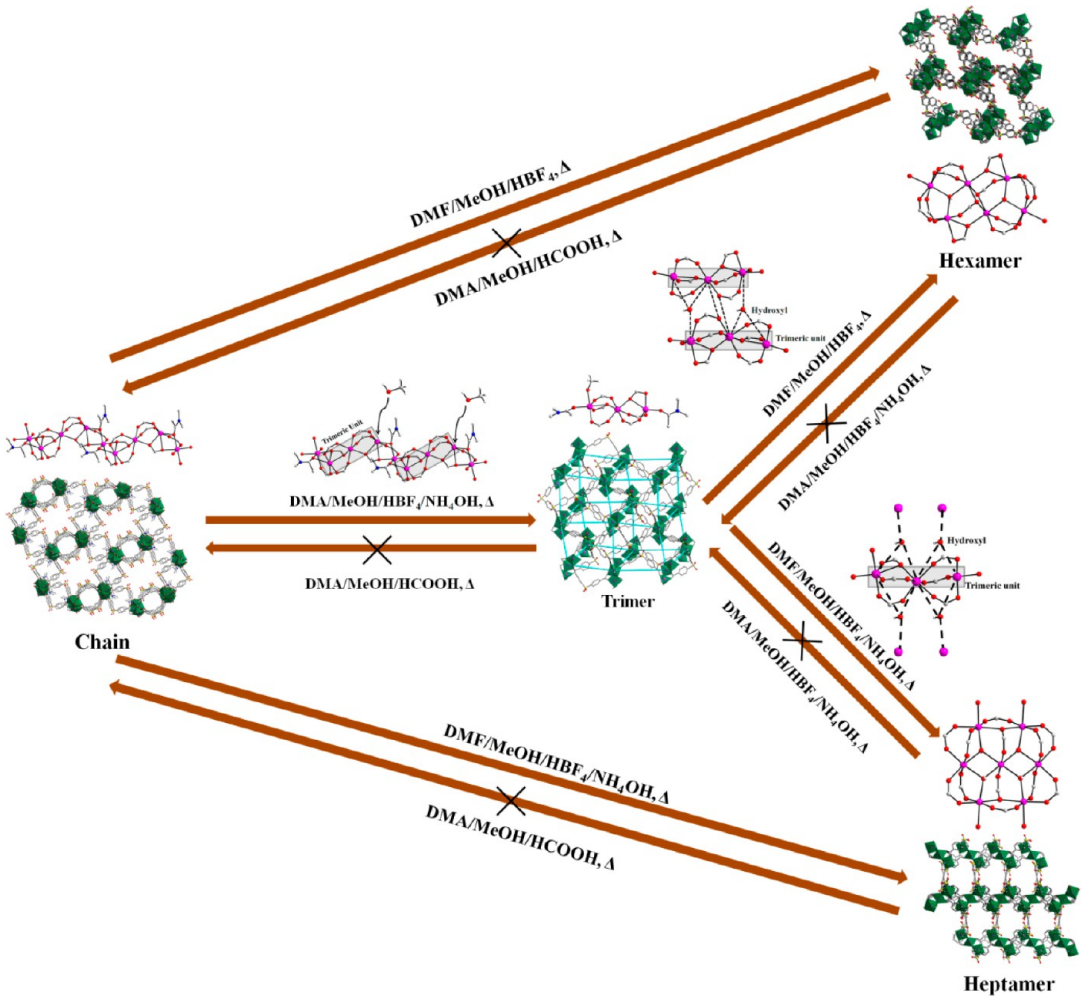

Figure 4. Schematic illustration of the transformation of **I** to **IIa** and the subsequent transformation of **IIa** to the compounds $[H_3O][Mn_3(\mu_3\text{-}OH)(C_{14}H_8O_6S)_3(H_2O)](DMF)_5$ and $[H_3O]_2[Mn_7(\mu_3\text{-}OH)_4(C_{14}H_8O_6S)_6(H_2O)_4](H_2O)_2(DMF)_8$, respectively[111] (see text).

WinGx package of programs.[21] The SQUEEZE program (WinGX platon program) was used to account for the disordered DMA molecules in **I**.[22] The SQUEEZE program, however, was not employed for the refinements of the compounds **IIa**–**e** and **III**. The details of structure determination are given in Table 2. Molecular formulas and weights have been corrected in Table 2, accounting for the excess thermally disordered carbon atoms in compounds **IIb**, **IIe**, and **III**, the unidentified lattice DMA molecules in compound **I** (as calculated from TGA, IR and CHN analysis), and the unidentified hydrogen atoms of solvent molecules in compound **IId**. The CCDC numbers of compound **I**–**III** are 1013589–1013595, respectively.

SPINEL OXIDE PREPARATION AND CHARACTERIZATION

The mixed metal MOF compound $[CoMn_2(C_{14}H_8O_6S)_3(DMA)_2(EtOH)]\cdot DMA$, **III**, was heated in air for 2 h at different temperatures (450 °C, 550 and 650 °C). After the heating, the resulting powdered product was characterized by PXRD, transmission electron microscopy (TEM), and magnetic studies. The morphologies and particle sizes of the product particles, formed after decomposition, were investigated using TEM (Hi tecnai; 300 kV) by mounting the samples on carbon coated copper grids. Surface areas of the samples were obtained by the BET method (Belsorp-Max), after preheating the samples at 200 °C for 4 h in dry N_2 atmosphere.

RESULTS AND DISCUSSION

Structure of $[Mn_4(C_{14}H_8O_6S)_4(DMA)_2]\cdot 3DMA$, I. The asymmetric unit of **I** has four Mn^{2+} ions that are crystallographically distinct [SI, Figure S6a]. All the Mn^{2+} ions are bonded with oxygen atoms and exhibit octahedral geometry, but with distortion. Thus, Mn(1) has six carboxylate oxygens, Mn(2) and Mn(3) have five carboxylate oxygens and a oxygen from the DMA molecules [O(10) and O(15), respectively], and Mn(4) has four carboxylate oxygens and two oxygens from the two coordinated DMA molecules. The Mn–O bond distances exhibit variations with values of 2.070(4)–2.493 Å. The average distances are 2.184 Å for Mn(1), 2.261 Å for Mn(2); 2.261 Å for Mn(3); 2.150 Å for Mn(4) (SI, Tables S2 and S3). The four $SDBA^{2-}$ anions also exhibit differences in their bonding behavior. Thus, the carboxylate oxygens of acid-1 and acid-3 exhibit $\mu_2\text{-}\eta^1\text{:}\eta^1$ mode, whereas acid-2 and acid-4 has one of the carboxylate groups coordinating in the $\mu_3\text{-}\eta^2\text{:}\eta^2$ mode, while the other carboxylate group coordinates in the $\mu_2\text{-}\eta^1\text{:}\eta^1$ mode (SI, Figure S6b). The Mn^{2+} ions are bonded through the carboxylate oxygens and the μ_2-O of the DMA molecules [O(10), O(15)] forming infinite Mn–O–Mn chains

DOI: 10.1021/ic5018517
Inorg. Chem. 2015, 54, 1254–1271

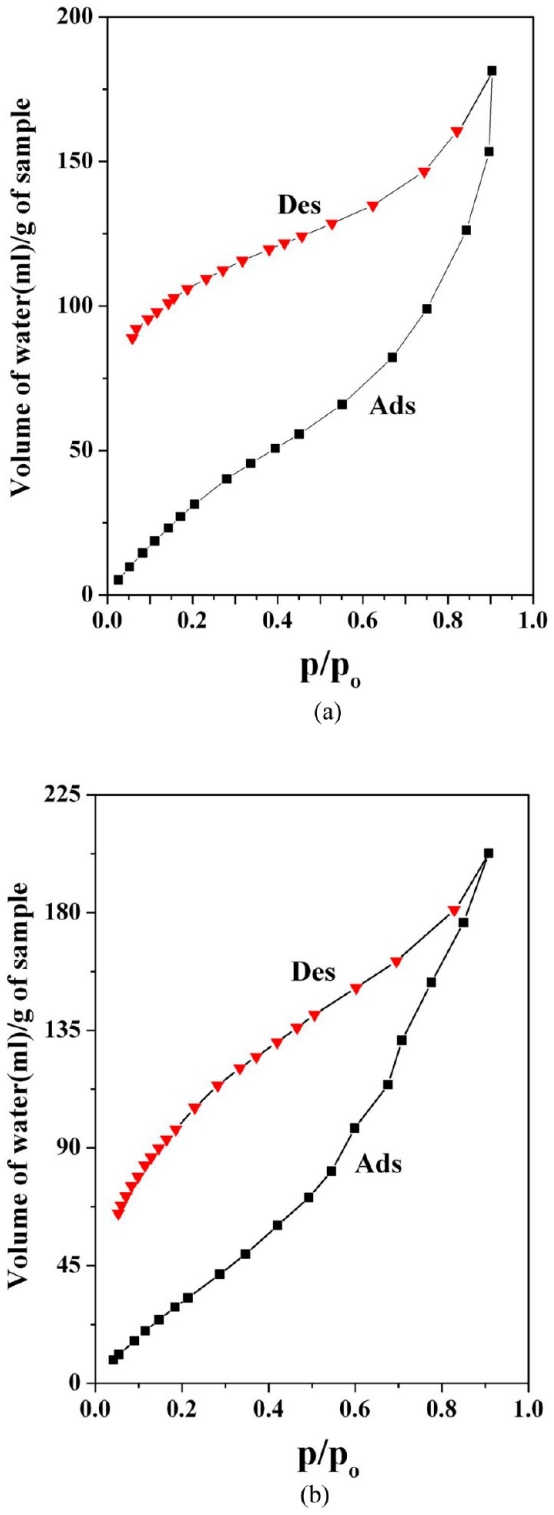

Figure 5. Adsorption–desorption isotherms of compound **I** using water (a) 298 K (b) 307 K.

(Figure 1a). The chains can be considered to be formed from trimeric $[Mn_3(CO_2)_6]$ units [Mn(1), Mn(2), and Mn(3)] connected by Mn(4) octahedra. The SDBA units links the Mn–O–Mn chains forming the three-dimensional structure consisting of one-dimensional channels along the 'a' direction (Figure 1b). The one-dimensional channels are decorated by the oxygen atoms of the sulfonyl groups of the $SDBA^{2-}$ anions.

Similar connectivity was also observed in $[Mn_2(hfbba)_2(bpy)]$,[23a] which also has trimeric $[Mn_3(CO_2)_6]$ units connected by an octahedral Mn^{2+} center. The difference between the two compounds is that the linear trimeric unit in $[Mn_2(hfbba)_2(bpy)]$[23a] consists of two trigonal bipyramidal units being connected to the distorted octahedral Mn^{2+} centers, while in **I** all the Mn^{2+} centers exist in distorted octahedral coordination geometry. Structurally, in $[Mn_2(hfbba)_2(bpy)]$[23a] each chain is connected to six chains forming a three-dimensional structure, whereas in **I**, each chain is connected to three other chains. Inorganic coordination polymers having one-dimensional manganese chains have been observed earlier (SI, Table S4).[23]

Structure of $[Mn_3(C_{14}H_8O_6S)_3(DMA)_2(MeOH)]\cdot DMA$, IIa. The asymmetric unit of compound **IIa** has three crystallographically independent Mn^{2+} ions [Mn(1), Mn(2) and Mn(3)], three $SDBA^{2-}$ anions, two coordinated and one lattice DMA molecule, and one coordinated methanol molecule [Mn(2)] [SI, Figure S7a]. Of the three Mn^{2+} ions, both Mn(1) and Mn(2) exhibit distorted octahedral geometry formed by the carboxylate oxygens of the $SDBA^{2-}$ anions [Mn(1)], and four carboxylate oxygens, one DMA oxygen atom and one oxygen of methanol [Mn(2)]. Mn(3), on the other hand, exhibits distorted square pyramidal geometry formed by the carboxylate oxygens and an oxygen atom of DMA [O(13)]. The Mn–O bond distances exhibit variations and have values of 2.039(2)–2.485(3) Å. The average distances are 2.178 Å for Mn(1); 2.203 Å for Mn(2); 2.153 Å for Mn(3). The selected bond distances and bond angles are given in the Supporting Information (SI, Tables S2 and S3). The oxygen atom [O(11)], belonging to methanol, participates in hydrogen bond interactions with the lattice DMA oxygen [O(22)] with an O···O contact distance of 2.750(4) Å and O – H···O bond angle of 155(4)° [SI, Table S5]. The three different $SDBA^{2-}$ ions show differences in their bonding behavior. Of the two carboxylate groups of acid-1 and acid-2, one coordinates with μ_2-η^2:η^1 mode, whereas the other coordinates with the μ_2-η^1:η^1 mode. Acid-3, on the other hand, coordinates in the μ_2-η^1:η^1 mode [SI, Figure S7b]. The Mn^{2+} ions form a trimeric unit $[Mn_3(CO_2)_6]$ as shown in Figure 2a. This trimer unit can be considered to be the secondary building unit for this structure. The connectivity between the trimer units and the $SDBA^{2-}$ anions initially forms a two-dimensional layer [Figure 2b], which are further bonded through $SDBA^{2-}$ anions leading to the formation of a three-dimensional structure [Figure 2c]. From a topological view, each Mn_3 cluster can be thought of as a node connected to six other clusters through $SDBA^{2-}$ anion linkers leading to a six connected *pcu* (primitive cubic) topology with a point symbol of $[4^{12}.6^3]$ [Figure 2c,d, SI Figure S7c)].[25]

The trimeric Mn^{2+} units, observed in the present structure, has also been observed in many manganese coordination polymers (SI, Table S6).[24] For example, in $Mn_3(bpdc)_3(DMA)_4$,[23c] the trimer units are formed from Mn^{2+} centers exhibiting octahedral coordination, whereas in **IIa**, one distorted square pyramidal and two distorted octahedral Mn^{2+} centers form the Mn_3 trimers. In both compounds, the connectivity between the trimeric units resembles a net with *pcu* topology.

Solvent Mediated Single Crystal to Single Crystal (SCSC) Transformations. Structural transitions involving phase changes have been investigated over the years to understand structure–property correlations.[26] SCSC trans-

DOI: 10.1021/ic5018517
Inorg. Chem. 2015, 54, 1254–1271

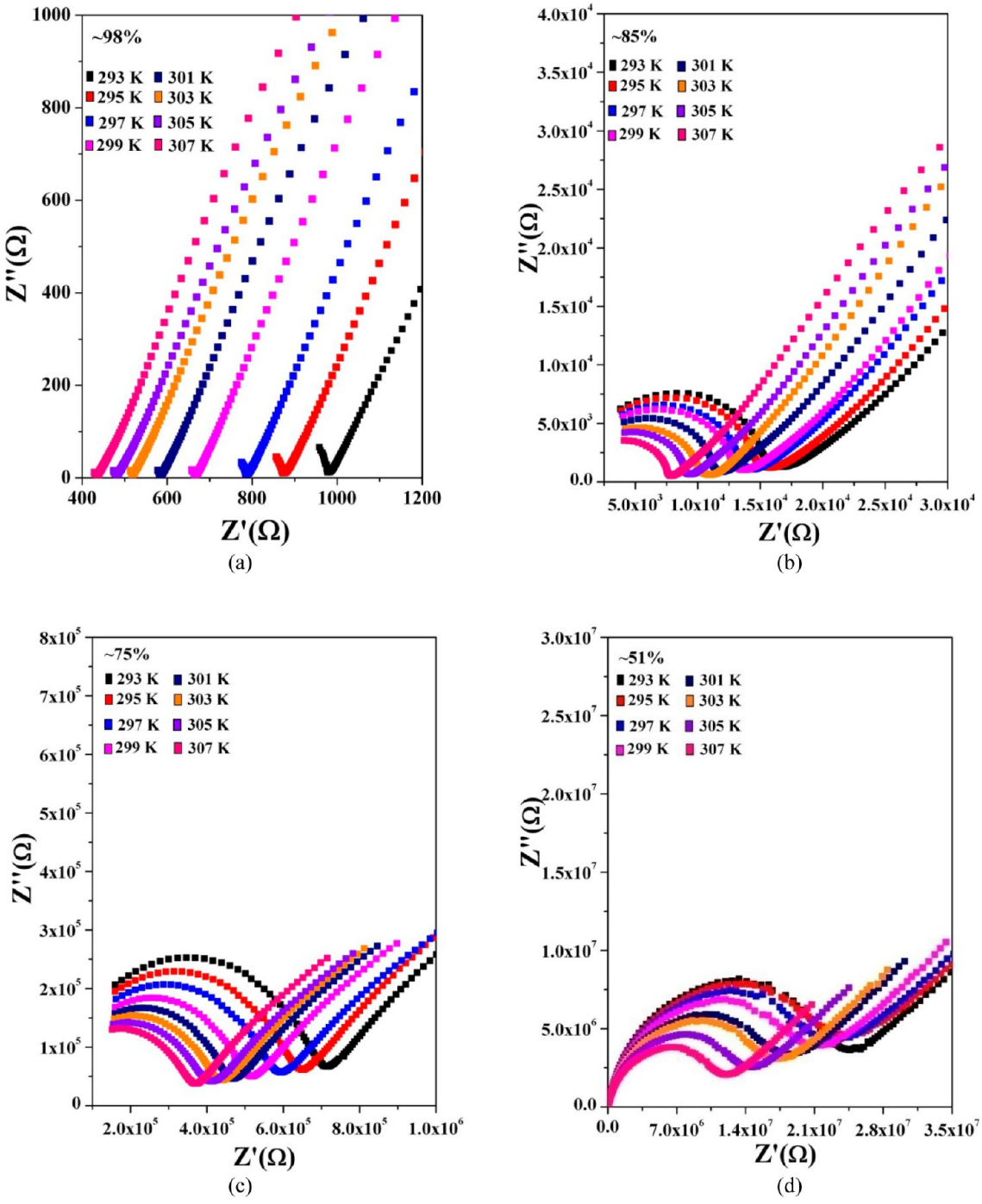

Figure 6. Experimental proton conductivity for **I** given as Nyquist plots at different temperatures (a) 98% (RH), (b) 85% (RH), (c) 75% (RH), and (d) 51% (RH).

Table 3. Variation of Proton Conductivity at Different Humidity Values for I

conditions	$[\sigma = \Omega^{-1}\ cm^{-1}]$	E_{act} = eV
34 °C and 98% humidity	0.87×10^{-3}	0.46
34 °C and 85% humidity	4.99×10^{-5}	0.42
34 °C and 75% humidity	1.09×10^{-6}	0.4
34 °C and 51% humidity	4.34×10^{-8}	0.4

formations in simple coordination complexes are also known.[27] The MOFs exhibiting different structures have provided another family of compounds for the study of SCSC transformations due to the flexible coordinations at the metal centers and structures. Thus, SCSC transformations employing heat,[28] light,[29] solvation/desolvation or rearrangement of enclosed guest molecules,[12−14] and postsynthetic metal ion exchange[30]/ligand exchange[31] have been investigated over the years. Many of the SCSC transitions in MOFs are accompanied by fascinating changes in physical and chemical properties such as improved framework stability for gas sorption,[30,31] magnetism,[28] catalytic reactions or the selective capture and separation of molecules,[13b,32,33] etc.

The presence of coordinated DMA as well as methanol groups in compound **IIa** encouraged us to explore the

DOI: 10.1021/ic5018517
Inorg. Chem. 2015, 54, 1254−1271

Table 4. Proton Conductivity and Activation Energy Values of the Known MOFs[a]

compounds	conductivity (Ω^{-1} cm^{-1})	activation energy (eV)	measurement conditions (°C, RH %)	reference
$[(Me_2NH_2)_3(SO_4)]_2[Zn_2(ox)_3]$	4.2×10^{-2}	0.129	25, 98	11a
PCMOF21/2	2.1×10^{-2}	0.21	85, 90	11b, 11c
$(NH_4)_2(adp)[Zn_2(ox)_3]\cdot 3H_2O$	8×10^{-3}	0.63	25, 98	11d
Ca-PiPhtA-NH_3	6.6×10^{-3}	0.40	24, 98	11e
Cd-5TIA	3.61×10^{-3}	0.16	28, 98	11f
$[\{(Zn_{0.25})_8(O)\}Zn_6(L)_{12}(H_2O)_{29}(DMF)_{69}(NO_3)_2]$	2.3×10^{-3}	0.22	RT, 95	11g
$(NH_4)_4[MnCr_2(ox)_6]\cdot 4H_2O$	1.7×10^{-3}	0.23	40, 96	11h
$Fe(ox)\cdot 2H_2O$	1.3×10^{-3}	0.37	25, 100	11i
$[Mn_4(SDBA)_4(DMA)_2]\cdot 3DMA$	0.87×10^{-3}	0.46	34, 98	this work
$[In(imdcH)(ox)]\cdot(NH_4)(H_2O)_{1.5}$	0.82×10^{-3}		23.5, 98.6	11j
[Zn(5-SipH)-(bpy)]·DMF·$2H_2O$	8.4×10^{-4}		25, 95	11k
$[H_3O]_2[Mn_7(\mu_3\text{-}OH)_4(SDBA)_6(H_2O)_4](H_2O)_2(DMF)_8$	3.44×10^{-4}	1.16	34, 98	11l
In-5TIA	5.35×10^{-5}	0.14	28, 98	11f
$[Zn(l\text{-}L_{Cl})(Cl)]\cdot H_2O$	4.45×10^{-5}	0.35	30, 98	11m
PCMOF-3	3.5×10^{-5}	0.17	RT, 98	11n

[a]ox = oxalate, adp = adipic acid, L = 1,3-bis(4-carboxyphenyl)imidazolium), SDBA = 4,4′-sulfonyldibenzoic acid, imdcH = imidazole-4,5-dicarboxylate, 5-SipH = 5-sulfoisophthalic acid, l-L_{Cl} = N-(4-pyridylmethyl)-L-valine.HCl

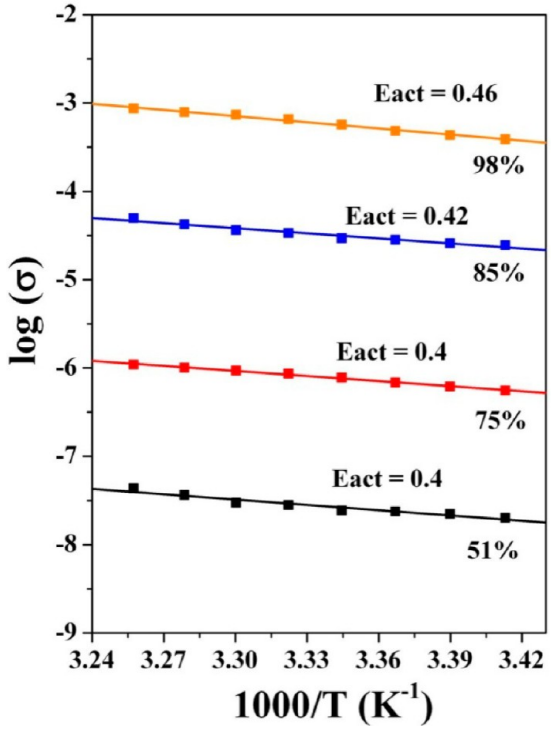

Figure 7. Activation energy for the proton conduction at different relative humidities for **I**.

possibility of investigating solution mediated SCSC transformation studies in this compound. It is likely that the coordinated solvent molecules could be replaced by other similar solvent molecules as such studies are known in MOFs.[13,14] To this end, single crystals of **IIa** were soaked in a mixture of DMA and various solvents for a period of 7−8 days. The single crystalline nature of the compound appears to be retained during the entire period of soaking of the crystals in the solvent mixture (Figure 3). A single crystal X-ray diffraction study of the resultant crystals proved unequivocally the substitution of the coordinated methanol group with the other $X_{solvent}$ molecules on the $Mn(2)^{2+}$ metal ion with minor changes in the coordination geometry. The complete substitution of the solvent molecules was subsequently corroborated by IR, TGA, and elemental analysis studies (SI). Solvent-mediated SCSC transformations of replacing coordinated solvents at the metal centers through simultaneous bond breaking and bond formation have been investigated before.[14c] Recently, the compound, $[Mn(L)(H_2O)](H_2O)1.5(DMF)$ {L = pyridine-4-yl-aminoisophthalate},[14b] was shown to undergo SCSC transformation involving the substitution of the coordinated water molecules by nitrile containing molecules such as acetonitrile, acrylonitrile, allylnitrile, or crotononitrile etc. without the loss of the single crystalline nature of the parent compound.

The structures of all the compounds **IIb**−**IIe** are similar, the only difference being in the coordinated solvent molecules along with minor differences in the overall coordination geometries of the metal ions. There are 86 non-hydrogen atoms in the asymmetric unit of **IId**, 87 in **IIb**, **IIc** and **III** and 88 in **IIe** (SI, Figure S8]. Similar to compound **IIa**, the asymmetric units contain three crystallographically independent Mn^{2+} ions [Mn(1), Mn(2), and Mn(3)], three $SDBA^{2-}$ anions, two coordinated and one lattice DMA molecule, and one coordinated $X_{solvent}$ (ethanol, acetonitrile, water, or ethylene glycol). The various coordination geometries adopted by the metal ions have been tabulated in Table S7. The structures are entirely consistent with that of **IIa**. Minor differences are observed in the coordination geometries adopted by $Mn(3)^{2+}$ ions in the compounds **IIb**−**IIe**. A distorted square pyramidal geometry was observed for $Mn(3)^{2+}$ in **IIc**−**IIe**, whereas a tetrahedral coordination geometry was observed in **IIb**.

As mentioned earlier, we have made attempts to partially substitute the manganese in **IIa** with other transition elements. To this end, we were successful in preparing a Co-substituted compound, **III**. The color of the crystals are dark blue as compared to the pale blue color of **IIa**, suggesting that cobalt has been incorporated in the lattice. A single crystal structural study on this compound reveals that the Co occupies a tetrahedral coordination similar to that observed for **IIb**. All the other structural parameters and details are similar to that observed in **IIa**.

The compounds **IIa** and **IIc**−**IIe** have five coordinated metal centers [Mn(3)]. The structural index parameter "τ", as

DOI: 10.1021/ic5018517
Inorg. Chem. 2015, 54, 1254−1271

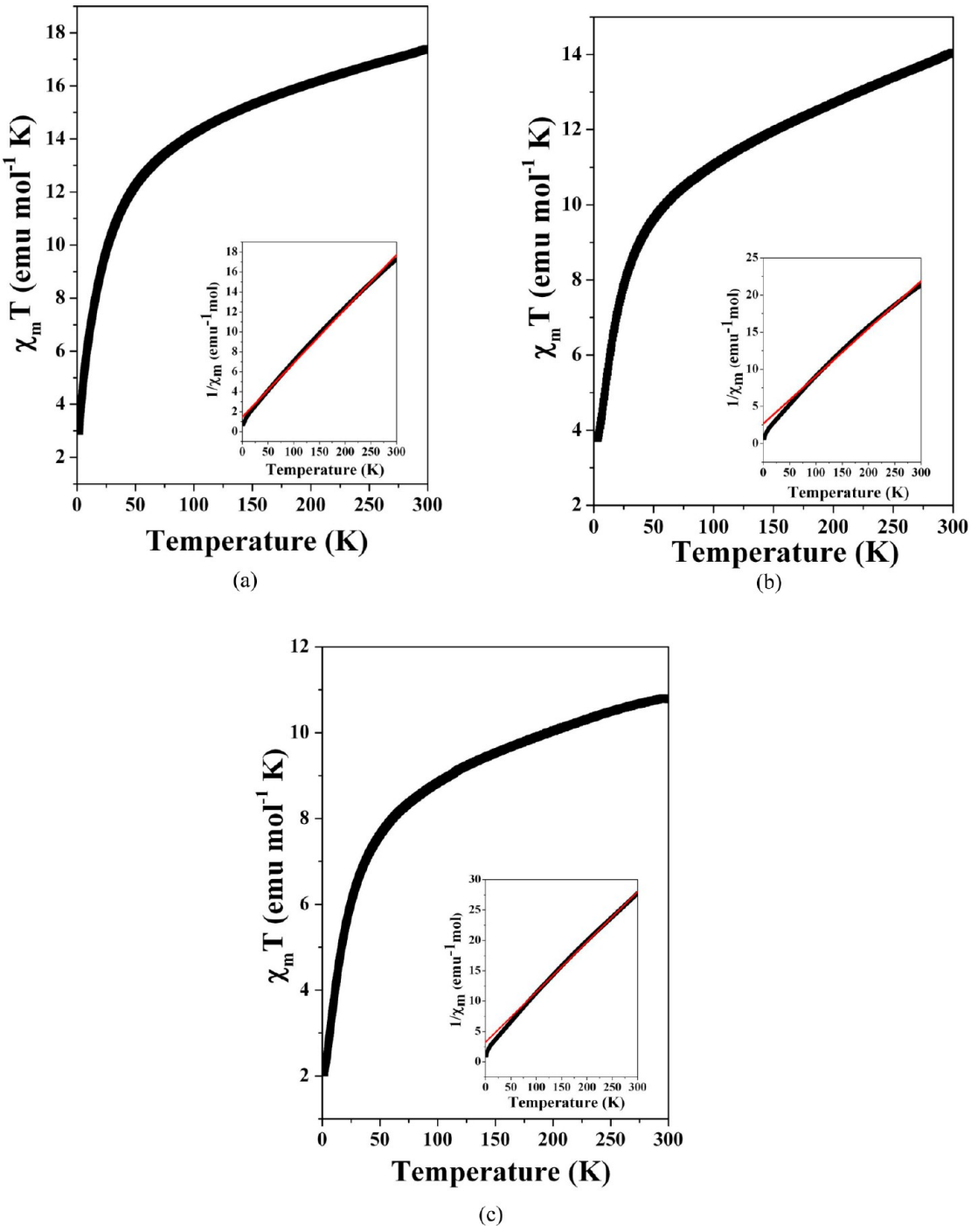

Figure 8. (a) The temperature variation of $\chi_m T$ of **I** ($1/\chi_m$ vs T plot is given as inset). (b) The temperature variation of $\chi_m T$ of **IIa** ($1/\chi_m$ vs T plot is given as inset). (c) The temperature variation of $\chi_m T$ of **III** ($1/\chi_m$ vs T plot is given as inset).

hypothesized by Addison and Rao, was calculated to rationalize and identify the formation of the geometry (the square pyramidal or the trigonal bipyramidal geometry) [SI, Table S8].[34] The overall structures are similar to the **IIa** structure.

Structural Transformation Studies. The one-dimensional chains of compound **I** and the Mn_3 clusters in compound **IIa** appear to have some resemblance as both have trinuclear oxo metal centers [Figures 1a and 2a and Table S7]. This prompted us to investigate the possible transformation between the two compounds. From the synthesis conditions (Table 1), the initial pH of the reaction mixture of compound **I** was higher than that for **IIa**: for **I**: pH = 3.3 and for **IIa**, pH = 2.1, while all other reaction conditions (temperature and time) were comparable (Table 1). The differences in the initial pH could be attributed to the lower pK_a value of formic acid (3.77) as compared to that of HBF_4 (−0.4) employed in the preparation of **I** and **IIa**, respectively.

In order to carry out the transformation reaction of **I** to **IIa**, compound **I** (0.15 g) was dispersed in a solvent mixture of DMA/methanol (6 mL/2 mL) followed by the addition of 0.06 mL of HBF_4 and 0.023 mL of NH_4OH to the mixture to reach the initial pH of 2.1. The mixture was then heated for varying

DOI: 10.1021/ic5018517
Inorg. Chem. 2015, 54, 1254−1271

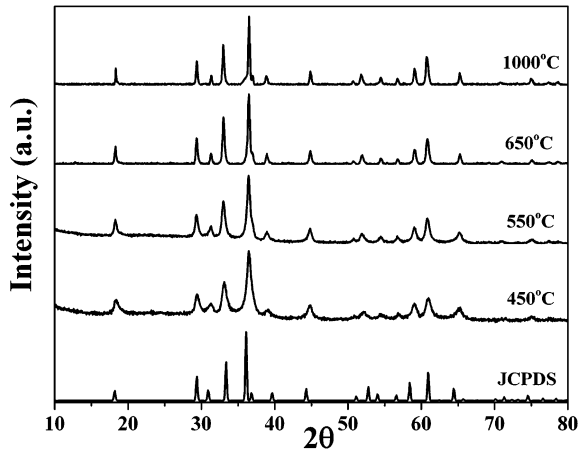

Figure 9. PXRD patterns of compound **III** heated at different temperatures (450−1000 °C).

Table 5. Preparation Conditions and Textural Characterizations of the Nanoparticles of the Spinel Oxides

temperature/time	particle size (XRD)/nm	particle size (TEM)/nm	surface area (BET)/$m^2\ g^{-1}$
450 °C/2 h	12.4	12.5 ± 2	30.1
550 °C/2 h	17	18 ± 3	28.7
650 °C/2 h	25.4	25 ± 2.7	13.6

periods of time at 90 °C. The products were filtered and analyzed using PXRD [SI, Figure S9(a)]. From the PXRD, it is clear that **IIa** starts to form after 2 h, and the entire transformation from **I** to **IIa** was complete in 10 h. The formation of **IIa** from **I** would require a dissolution and recrystallization pathway as the trimer units are similar in both the compounds. As can be noted, in **I** the trimer units are connected through a fourth manganese ion (Figure 1a) forming the infinite Mn−O−Mn chains. The lowering of the pH probably helped in breaking the chain to smaller units. During the course of the transformation reaction, the methanol molecule, employed as the solvent, binds with the Mn center. A schematic of the possible pathway is given in Figure 4. Attempts to transform compound **IIa** to **I** by heating **IIa** in a mixture of DMA/methanol/formic acid (6 mL/2 mL/0.02 mL, initial pH = 3.3) even at 110 °C was not successful [SI, Figure S9b].

Previously, we have prepared and characterized two Mn-containing compounds $[H_3O][Mn_3(\mu_3\text{-}OH)(C_{14}H_8O_6S)_3(H_2O)](DMF)_5$, **A** and $[H_3O]_2[Mn_7(\mu_3\text{-}OH)_4(C_{14}H_8O_6S)_6(H_2O)_4](H_2O)_2(DMF)_8$, **B** having Mn_6 and Mn_7 cluster core.[111] The Mn_3 trimer in $[Mn_3(C_{14}H_8O_6S)_3(DMA)_2(EtOH)]\cdot DMA$, **IIa**, appears to have some resemblance to the Mn_6 and Mn_7 clusters. It occurred to us whether the trimer compound (**IIa**) could be employed as the starting material for the preparation of the Mn_6 and Mn_7 cluster compounds. Thus, compound **IIa** (0.12 g) was heated at 90 °C in a mixture of DMF/methanol/HBF_4 (6 mL/2 mL/0.06 mL, initial pH = 1.5) as the solvent. We observed that the compound **IIa** dissolves completely at 90 °C forming a clear solution. After 24 h of reaction at 90 °C, we observed the formation of a white colored solid, which was filtered and dried. The PXRD studies of the white compound revealed that it is the hexameric manganese compound, $[H_3O][Mn_3(\mu_3\text{-}OH)(C_{14}H_8O_6S)_3(H_2O)](DMF)_5$[111] [SI, Figure S9c]. It is clear that the transformation is through a dissolution and recrystallization pathway.

When compound **IIa** was heated at 90 °C in the same solvent mixture along with the addition of a few drops of NH_4OH (0.023 mL, initial pH = 2.1), the heptanuclear compound $[H_3O]_2[Mn_7(\mu_3\text{-}OH)_4(C_{14}H_8O_6S)_6(H_2O)_4](H_2O)_2(DMF)_8$[111] started to form after 2 h, as revealed by the PXRD studies, and the transformation was complete after 12 h of heating [SI, Figure S9d].

A schematic of the possible pathway of the formation of the Mn_6 and the Mn_7 compounds from the Mn_3 compound (**IIa**) is given in Figure 4. We also made attempts to convert both the Mn_6 and Mn_7 compounds back to the Mn_3 compound **IIa**. We employed a reaction condition having the Mn_6/Mn_7 cluster compounds in a mixture of DMA/methanol/HBF_4/NH_4OH (6 mL/2 mL/0.06 mL/0.023 mL, initial pH = 2.1) and heated at 110 °C. In spite of our best efforts, the reverse reaction appears to be not feasible [SI, Figure S9e].

Since the trimer compounds $[Mn_3(C_{14}H_8O_6S)_3(DMA)_2(X_{solvent})]\cdot DMA$, **II**, appear to have part of the Mn_6 and Mn_7 cluster connectivity and the one-dimensional chains in compound **I** have similar trinuclear Mn-oxo units as observed in compound **II**, we envisaged the possible utilization of compound **I** as a starting material for the preparation of the Mn_6 and Mn_7 cluster compounds directly. Thus, when compound **I** was heated at 90 °C in a mixture of DMF/MeOH/HBF_4 (6 mL/2 mL/0.06 mL, initial pH = 1.5), we observed that compound **I** dissolves completely forming a clear solution. After 36 h of heating at 90 °C, we observed the formation of a white colored solid which was filtered and dried. The PXRD of the white compound was found to be that of the Mn_6 cluster compound $[H_3O][Mn_3(\mu_3\text{-}OH)(C_{14}H_8O_6S)_3(H_2O)](DMF)_5$[111] [SI, Figure S9f]. When compound **I** was dispersed in a solvent mixture of DMF/MeOH/HBF_4/NH_4OH (6 mL/2 mL/0.06 mL/0.023 mL, initial pH = 2.1) and heated at 90 °C, the Mn_7 cluster compound $[H_3O]_2[Mn_7(\mu_3\text{-}OH)_4(C_{14}H_8O_6S)_6(H_2O)_4](H_2O)_2(DMF)_8$[111] started to form after 6 h and the entire transformation was complete after a period of 30 h [ESI, Figure S9(g)]. Attempts to transform the Mn_6 and the Mn_7 compounds to compound **I** by heating in a mixture of DMA/methanol/formic acid (6 mL/2 mL/0.02 mL, initial pH = 3.3) even at 110 °C was not successful. [SI, Figure S9h,i].

Thermal Stability. The thermogravimetric analysis (TGA) was used to investigate the thermal stability of the compounds [SI, Table S9, Figure S10]. The conditions for the TGA studies are T_{range} = 30−850 °C; heating rate = 5 °C min^{-1}; gas flow rate = 20 mL min^{-1} (air). Compound **I** exhibited three distinct weight losses. The first weight loss of ∼13.4% (T_{range} = 50−210 °C) corresponds to the loss of three DMA molecules (calc. 13.9%). The second gradual weight loss of ∼8.9% (T_{range} = 210−380 °C) corresponds to the loss of the two coordinated DMA molecules (calc. 9.3%). The final weight loss of ∼59% (T_{range} = 380−530 °C) corresponds to the loss of the $SDBA^{2-}$ (calc. 58.6%). Similar experimental conditions were maintained for the study of other compounds as well. Thus, two losses were observed in the TGA studies of the compounds **IIa** and **III**. The first loss of ∼20.5% for **IIa** and ∼22.2% for **III** (T_{range} = 200−300 °C) corresponds to the loss of the coordinated and lattice DMA molecules along with the coordinated $X_{solvent}$ molecules (Calc. 21.4% for **IIa** and 22.1% for **III**). The second and final weight loss of ∼60.2% for **IIa** and 58.3% for **III** (T_{range} = 380−470 °C) corresponds to the loss of

DOI: 10.1021/ic5018517
Inorg. Chem. 2015, 54, 1254−1271

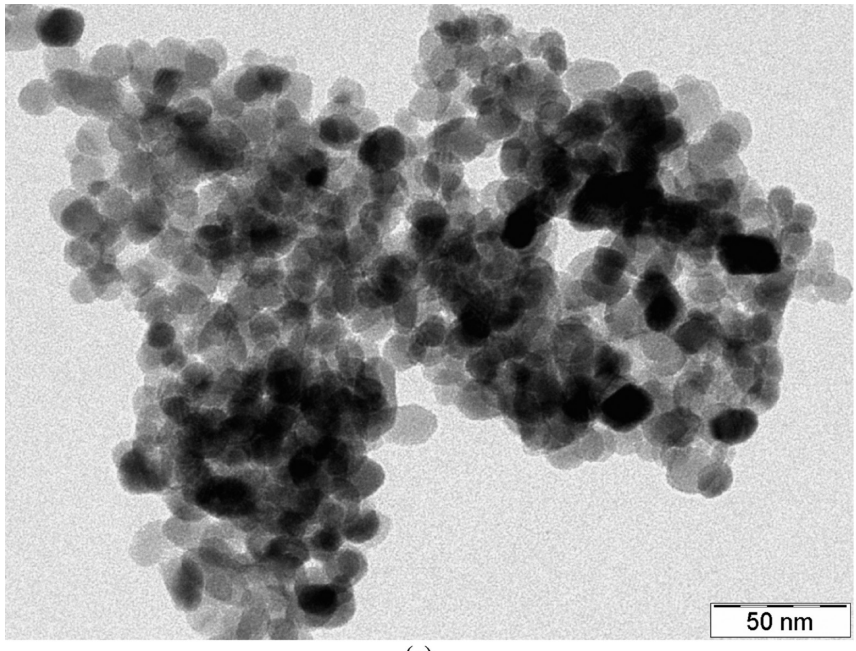

(a)

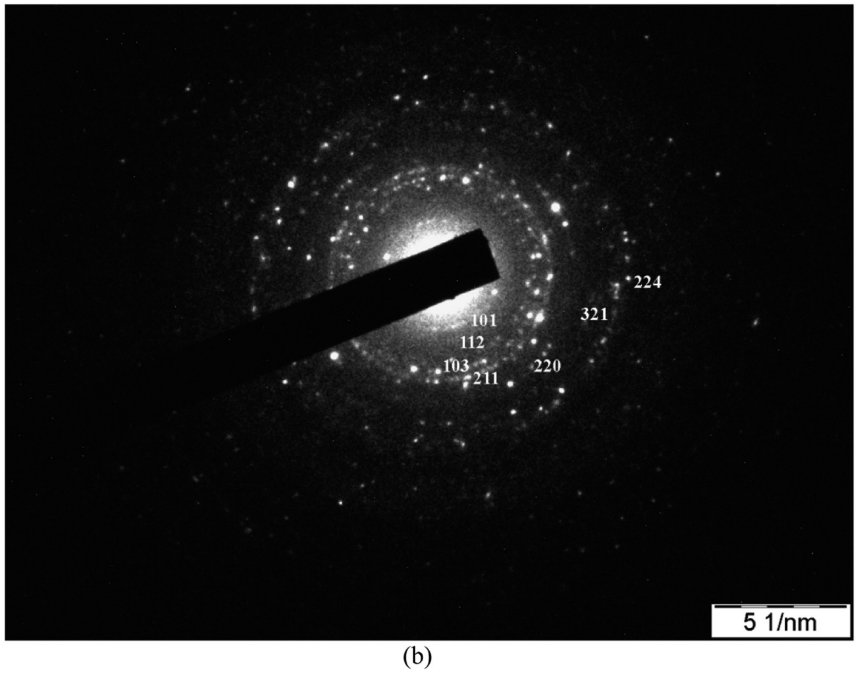

(b)

Figure 10. (a) TEM image of the particles of $CoMn_2O_4$ spinel prepared at 450 °C. (b) Selected area electron diffraction (SAED) of a particle at 450 °C.

the $SDBA^{2-}$ (calc. 59.9% for **IIa** and 59.2% for **III**). The PXRD studies of the products, after the TGA studies, revealed the formation of a mixture of Mn_2O_3 (JCPDS: 89-4836) and Mn_3O_4 (JCPDS: 24−0734). Compound **III**, on the other hand, formed the spinel phase $CoMn_2O_4$ (JCPDS: 77-0471).

TGA and PXRD studies were employed to understand the effects of guest molecules removal/reinsertion in **I**. To this end, the as-synthesized compound **I** was heated to 180 °C for 1 h. to remove the solvent molecules and then resolvated by immersing in DMA at 80 °C. TGA studies were then carried out on the preheated (180 °C/1h) sample as well as the resolvated samples. The desolvated compound of **I** did not exhibit any initial weight loss during the TGA investigations [SI, Figure S11]. A small gradual weight loss of ∼10.3% was observed (T_{range} = 250−380 °C), which corresponds to the loss of two coordinated DMA molecules (expected weight loss = 10.8%). From this study, one can infer that the preheating (180 °C/1h) of **I** appears to remove only the lattice DMA molecules and not the coordinated ones. The larger weight loss of ∼69% corresponds to the loss of four $SDBA^{2-}$ ions (calc. = ∼68.1%).

DOI: 10.1021/ic5018517
Inorg. Chem. 2015, 54, 1254−1271

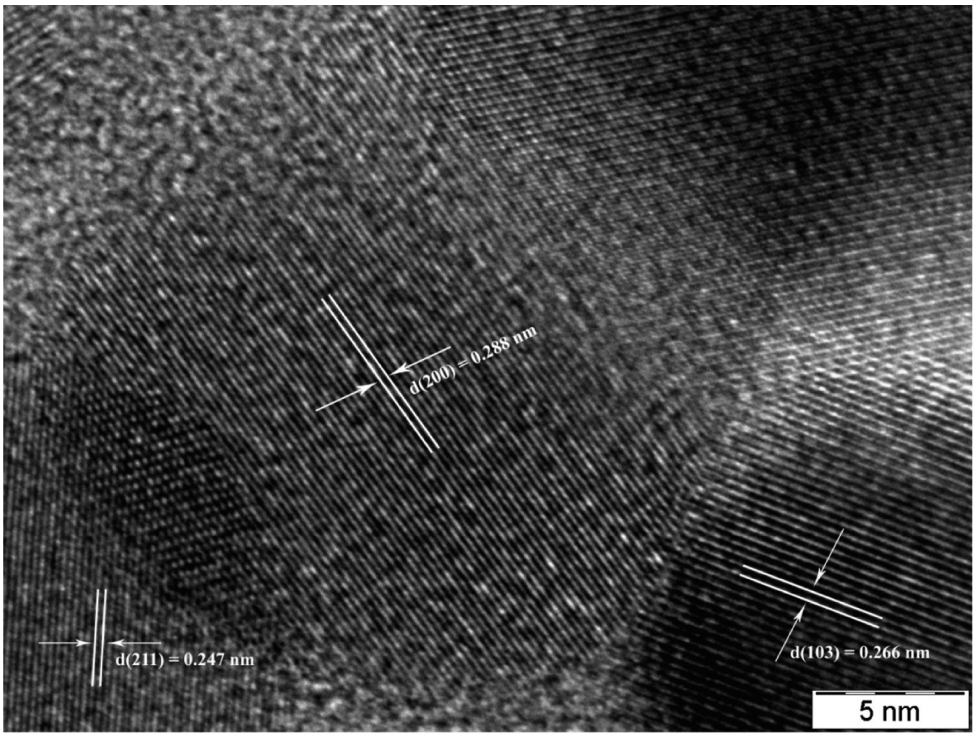

Figure 11. High resolution transmission electron microscopy (HRTEM) image of a particle at 1000 °C (bulk).

TGA study on the resolvated compound, on the other hand, exhibits a behavior which is almost similar to the as-synthesized compound. This study suggests that the lattice DMA molecules are labile and can be reversibly removed. The PXRD patterns of the desolvated compound shows reasonable framework stability with only a small loss of crystallinity, which appears to be regained during the resolvation step [SI, Figure S12]. A Le Bail fit of the PXRD pattern of the desolvated compound shows that the structural integrity of the compound is retained. We have, however, observed a reduction in the unit cell parameters and cell volume, which may be attributed to the loss of the guest DMA molecules from the channels of compound **I** [SI, Figure S13].

Water Absorption. The removal of lattice DMA molecules from **I** was established using the TGA and PXRD studies. This encouraged us to investigate the possibility of replacing the lattice DMA molecules with water molecules. To this end, compound **I** was taken in the TGA setup and heated to 180 °C (N_2 atmosphere, flow = 50 mL/min). The samples were cooled under the flow of nitrogen gas, and then the nitrogen was allowed to bubble through distilled water and pass over the samples for 60 min. During this process, we observed a partial reabsorption of water molecules. A gain in weight of 4.5% was absorbed from the dehydrated weight of ∼84.2%. This would correspond to ∼5 mol of water per mole of **I** [SI, Figure S14]. The relatively low water uptake in **I** during the TGA studies prompted us to take up water sorption behavior employing a BELSORB aqua equipment, which would have a controlled water dosages over dehydrated samples.

To investigate the water sorption behavior, the sample of **I** was preheated at 180 °C for 1 h. The water sorption isotherm studies were carried out at 298 K, which indicated a gradual water uptake with values reaching to 181 mL/g at p/p_0 = 0.9 [Figure 5a]. This value of water uptake appears to be equivalent to ∼12.5 mol H_2O/mol of **I**. The slow dosage of water, employing the BELSORB Aqua equipment, was carried out over a period of 35 h. A hysteretic behavior was also observed in the adsorption−desorption cycles, which suggests the presence of hydrophilic channels in the structure. PXRD pattern of compound **I** after the water adsorption experiment did not reveal any significant changes indicating the stability of compound **I** in an atmosphere of water vapor [SI, Figure S12]. It may be noted that a long exposure to water vapor may be required for the complete uptake of the water molecules in **I**. The water sorption studies were also carried out at a slightly elevated temperature of 307 K for **I** [Figure 5b]. A slow and gradual water uptake of 203 mL/g at p/p_0 = 0.9 was observed. This value is comparable to the water uptake at room temperature and corresponds to ∼14 mol H_2O/mol of **I**. In the present experiment, we observed that the hysteresis loop does not make a closure even when the partial pressures were close to zero. This behavior could be attributed to irreversible adsorption of water molecules within the pores at the particular adsorption temperature.[2f]

Proton Conductivity. The water adsorption and TGA studies indicated the possibility of replacing the DMA molecules with water. The water adsorption studies also indicated the presence of ∼12.5 mol of water molecules per mole of **I** within the channels. Thus, the likely presence of hydrophilic channels along with sulfonyl groups of the $SDBA^{2-}$ anions prompted us to investigate the possibility of proton migration in **I**. A frequency range of $0.1-10^6$ Hz with signal amplitude of 0.12 V was employed to scan the samples employing the ac-impedance spectroscopy studies (Alpha, Novocontrol). For this experiment, pellets of **I** were held in place using two stainless-steel electrodes. An indigenously fabricated cell was employed to expose the sample to varying humidities and temperatures. Before the proton conductivity experiments, the compound was exposed to and equilibrated at respective humidity values for 24 h. The PXRD of the samples,

DOI: 10.1021/ic5018517
Inorg. Chem. 2015, 54, 1254−1271

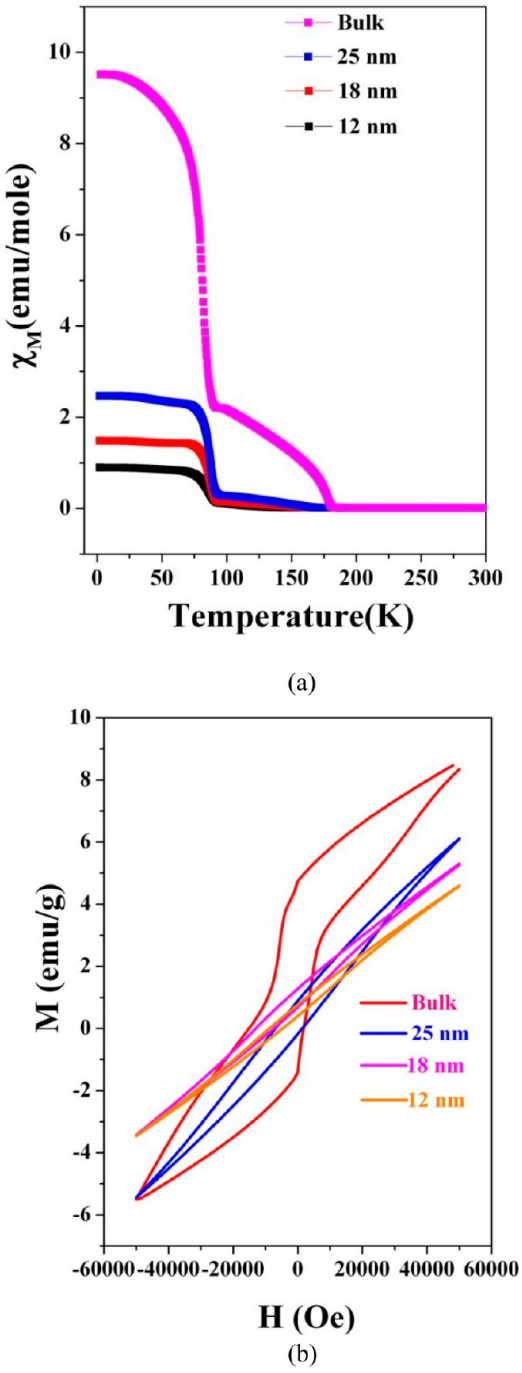

Figure 12. (a) The temperature dependence of χ_M (H = 100 Oe) (FC) for different sized $CoMn_2O_4$ nanoparticles along with the bulk. (b) M vs H plots of the different sized $CoMn_2O_4$ nanoparticles along with the bulk sample.

after exposure to different humidity values, did not exhibit any noticeable changes suggestive of degradation in the crystallinity [SI, Figure S15].

The proton conductivity studies gave values of 0.87×10^{-3} Ω^{-1} cm^{-1} (34 °C and 98% RH) [Figure 6a, Table 3]. The conductivity value observed in **I** is similar to the conductivity value observed in the porous indium MOF $[In(imdcH)(ox)]\cdot(NH_4)(H_2O)_{1.5}$ {imdcH = 4,5-imidazoledicarboxylate, ox = oxalate, $\sigma = 0.82 \times 10^{-3}$ Ω^{-1}cm^{-1} at 98.6% RH and 23.6 °C}[11j] and is also comparable to the other good proton conducting MOF compounds reported before [Table 4].[11] Proton conductivity studies also reveals marked dependence of the conductivity values on the relative humidity, the values decreasing with decreasing relative humidities. Thus, conductivity values in the range of $\sim 10^{-5}$ Ω^{-1} cm^{-1} at 85% RH, $\sim 10^{-6}$ Ω^{-1} cm^{-1} at 75% RH and $\sim 10^{-8}$ Ω^{-1} cm^{-1} at 51% RH were noted for compound **I** at 34 °C [Table 3]. The activation energies, observed at different relative humidities, are comparable with values of 0.4 eV for 51 and 75% RH, 0.42 eV for 85% RH, and 0.46 eV for 98% RH [Table 3, Figure 7]. The observed proton conductivity values suggest the possibility of the Grotthus mechanism in the compound (0.1−0.5 eV).[2a,35] The marginally larger activation energies observed at higher humidity values suggest the possibility of additional processes along with the Grotthus mechanism. It is likely that at higher humidities the water molecules could also become the vehicles for the migration of protons, which could have contributed to the higher observed activation energies.[11d] The proton conductivity value observed at 34 °C and 98% RH for compound **I** is higher than that observed in two other similar proton conducting Mn-MOFs, $[H_3O][Mn_3(\mu_3\text{-}OH)(C_{14}H_8O_6S)_3(H_2O)](DMF)_5$, ($3 \times 10^{-4}$ Ω^{-1} cm^{-1} at 34 °C and 98% RH), and $[H_3O]_2[Mn_7(\mu_3\text{-}OH)_4(C_{14}H_8O_6S)_6(H_2O)_4](H_2O)_2(DMF)_8$ (3.44×10^{-4} Ω^{-1} cm^{-1} at 34 °C and 98% RH).[11i]

Magnetic Behavior. The magnetic behavior of the prepared compounds was investigated employing a SQUID magnetometer in the temperature range 2−300 K, and the results are presented in Figure 8. As compounds **IIa**−**IIe** have the same structures, the magnetic behavior of only **IIa** is presented here. For the compounds **I**, **IIa**, and **III**, an overall antiferromagnetic behavior was observed. The $\chi_M T$ values per Mn_4 unit in **I**, Mn_3 units in **IIa**, and $CoMn_2$ unit in **III**, at room temperature, were found to be 17.4 (**I**), 14.1 (**II**), and 10.8 (**III**) emu mol^{-1} K, respectively. These values are close to the expected spin only $\chi_M T$ values of 17.6 (**I**) 13.1 (**II**) and 10.6 (**III**) emu mol^{-1} K (S = 5/2 for high spin Mn^{2+} and S = 3/2 for high spin Co^{2+}). This indicates negligible orbital contribution to the overall magnetic moment in all the compounds. The absence of long-range magnetic ordering was established as no divergence was noted in the field-cooled (FC) and the zero-field cooled (ZFC) magnetic susceptibility values as a function of temperature (SI, Figure S16). From a Curie−Weiss fit of the $1/\chi_M$ vs T plot (75−300 K), θ_p values of −26.7 K (**I**), −41.2 K (**II**), and −39 K (**III**) were obtained. The values of θ_p being negative suggests the possibility of antiferromagnetic interactions between the manganese centers.

From the structural description, it is clear that the triuclear manganese units in both compounds **I** and **IIa** are formed with —Mn−O—C−O—Mn— and —Mn−O—Mn— connectivities. The magnetic behavior of the compounds, thus, would depend on the nature of these bonds (bridging modes of the carboxylates as well as the bridging angles of the —Mn−O—Mn— bridges). According to Goodenough and Kanamori rules,[36a] ferromagnetic coupling may be expected if the Mn−O—Mn angle is ∼90°, and strong antiferromagnetic exchanges are expected when the Mn−O—Mn angle is ∼180°. In the case of the carboxylate bridging, the syn−syn and the anti−anti bridging modes exhibit an antiferromagnetic behavior as compared to the syn−anti bridging mode, which could be ferromagnetic.[36b,c] In **I**, the trinuclear Mn_3 units have syn−syn carboxylate bridges, and the Mn−O—Mn angle is ∼107.7°. This suggests a dominant antiferromagnetic coupling within the trinuclear units. The trimer units are connected through

DOI: 10.1021/ic5018517
Inorg. Chem. 2015, 54, 1254−1271

octahedral Mn^{2+} with a Mn−O−Mn angle of ∼97°, which could lead to ferromagnetic exchanges. It is likely that the antiferromagnetic exchanges within the trinuclear unit are much stronger as compared to the ferromagnetic ones and gives rise to an overall antiferromagnetic behavior in **I**. Similar magnetic behavior has been observed before.[24a] In **IIa**, the trinuclear Mn_3 units have syn−syn carboxylate bridges and the Mn−O—Mn bond angles have values of 108.2° and 103.8°, which would support antiferromagnetic interactions between the Mn^{2+} centers within the Mn_3 trimers. Similar magnetic behavior has been observed in most of the one-dimensional Mn chain containing coordination polymers as well as trinuclear Mn clusters (Tables S4 and S6).

Thermal Decomposition Studies and Formation of Spinel Oxide Nanoparticles. The PXRD patterns after the TGA study on the mixed metal compound **III** clearly revealed the formation of the $CoMn_2O_4$ spinel phase. This also gave us an idea that **III** could be a single source precursor for the preparation of functional ceramic oxides. We wanted to understand the decomposition behavior of the mixed metal MOF carefully to learn of the possibility of forming such mixed metal ceramic oxides with smaller particle sizes. Our earlier studies in this direction resulted in forming similar oxides with nanometer range particles.[15] To this end, the mixed metal MOF compound $[CoMn_2(C_{14}H_8O_6S)_3(DMA)_2(EtOH)]\cdot$ DMA, **III**, was heated, ex-situ, in air at different temperatures (450, 550, and 650 °C) for 2 h each, and the products of decomposition were characterized by PXRD studies [Figure 9]. The PXRD patterns indicated the formation of the pure tetragonal structure of mixed metal oxide $CoMn_2O_4$ (JCPDS 77-0471). The products have Mn^{3+} in the structure which indicates that the Mn^{2+} ions are oxidized to Mn^{3+} ions during the decomposition in air. The XRD peaks are broad when the sample was heated at 450 °C. On heating further, the XRD peaks expectedly become more sharper and the corresponding intensity increases. This suggests that the particle sizes of the decomposed product could be increasing. The (211) peak in the PXRD pattern was fitted employing the Debye−Scherrer formula to obtain the average particle size of the spinel oxide products [Table 5].[37] The fit suggested that the spinel oxides have small particle sizes (12.4 nm at 450 °C, 17 nm at 550 °C, and 25.4 nm at 650 °C). This calculated particle sizes from the XRD studies also correlated well with the TEM studies: 12.5 nm (450 °C), 18 nm (550 °C) and 25 nm (650 °C). The TEM studies also confirmed spherical particles for the spinel oxide [Figure 10a, Table 5, SI Figures S17, S18]. The TEM image along with the selected area electron diffraction (SAED) pattern of $CoMn_2O_4$ (450 °C) is shown in Figure 10. As can be seen, the single particle can be indexed to the tetragonal $CoMn_2O_4$ phase [Figure 10b]. The sample heated at 1000 °C has very sharp PXRD lines (Figure 9), which suggests that the particles must have sintered and formed large agglomerates. A HRTEM image of the sample shows good lattice fringes and can be indexed to the tetragonal spinel phase (Figure 11). The TEM images also indicated that the particle sizes of the $CoMn_2O_4$ phase increase with the increase in temperature. Energy dispersive X-ray spectroscopy (EDS) analysis on the samples [SI, Figure S19] indicated a Co:Mn ratio of 1:2. The adsorption studies of the different $CoMn_2O_4$ samples along with the BET plots of the isotherms indicated that with increasing particle sizes, the surface area decreases (30.1 $m^2\ g^{-1}$ for the 12.5 nm particles to 13.6 $m^2\ g^{-1}$ for the 25 nm particles) [SI, Figure S20, S21, Table 5]. Similar observations were reported earlier.[38]

Magnetic Behavior of the $CoMn_2O_4$ Nanoparticles. Size-dependent magnetic behavior has been observed, especially in many nanosystems involving metal, metal-oxides, and related compounds.[39a−d] During the current study, we have prepared $CoMn_2O_4$ compounds with different particle sizes. It would be interesting to investigate the magnetic behavior of such compounds with small particle sizes. We have carried out the magnetic susceptibility studies on all the compounds including the bulk $CoMn_2O_4$ with an applied magnetic field of 100 Oe [Figure 12a]. The bulk $CoMn_2O_4$ exhibited two incongruities, one at 180 K and the other at 90 K. Magnetic and neutron diffraction studies carried out on bulk $CoMn_2O_4$ samples, however, exhibited only one transition at 100 K.[39e] The observed transition at 180 K in the present study may be due to the presence of a small amount of an impurity phase (∼5%), which is related to the $Co_xMn_{3-x}O_4$. Since Mn_3O_4 as well as $CoMn_2O_4$ have the spinel structure, it would be difficult to detect the presence of the substituted Mn_3O_4 related phase employing PXRD (Figure 9).[40] In addition, the likely amount of impurity (∼5%) could be in the range of the limits of detection by laboratory X-ray diffraction methods. The high temperature magnetic transition (180 K) appears to get suppressed as a function of particle sizes (from the bulk to the nanoparticle), which suggests that the impurity phase may not be present in the smaller particles of $CoMn_2O_4$.

The ferromagnetic transition observed at low temperatures in the bulk as well as the nanoparticle phases could be attributed to the existence of a multidomain structure within the $CoMn_2O_4$ spinel. Large differences in susceptibility values could also be seen above and below the transition temperature (90 K). Near 90 K, the bulk sample, as well as the nanoparticle samples, exhibits the largest changes in the susceptibility. The change in susceptibility values decrease with the decrease in particle sizes. The differences in the susceptibility values of the nanoparticles could be attributed to the variations in particle sizes as well as the suppression of the impurity phases with decreasing particle sizes.[15a] The different particle sizes of the $CoMn_2O_4$ does not appear to have any effect on the calculated effective magnetic moment values (μ_{eff}), which were found to be in the range 7.3−7.6 μ_B. For the $CoMn_2O_4$, a spin only value of 7.94 μ_B would be obtained with Co^{2+} ions in the tetrahedral site and the Mn^{3+} ions in the octahedral sites. The present μ_{eff} values appear to be comparable with the spinel oxide.

To understand the magnetization behavior, the M vs H studies were performed on both the bulk as well as the $CoMn_2O_4$ nanoparticles. The M(H) curve of the bulk sample measured at 2 K shows a large hysteresis without saturation confirming the ferromagnetic nature of the compound [Figure 12b]. For the nanoparticles, the decrease in particle sizes from 25 to 12.5 nm leads to a decrease in the remnant field and coercivity (and consequently a smaller hysteresis), which might suggest a long-range ferrimangnetic ordering. It may be noted that an almost linear $M(H)$ curve was observed for the smallest particle size (12.5 nm). Similar behavior was observed earlier.[15]

CONCLUSIONS

In conclusion, two new three-dimensional manganese compounds, $[Mn_4(C_{14}H_8O_6S)_4(DMA)_2]\cdot 3DMA$, **I** and $[Mn_3(C_{14}H_8O_6S)_3(DMA)_2(MeOH)]\cdot DMA$, **IIa**, consisting of Mn−O−Mn chains (**I**) and trinuclear manganese units (**IIa**), coordinated by carboxylate groups and different solvents, have

DOI: 10.1021/ic5018517
Inorg. Chem. 2015, 54, 1254−1271

been synthesized and characterized. Solvent-mediated SCSC transformation studies has also been accomplished. Structural transformation studies reveal that **I** can be converted to **IIa** through a simple manipulation of the reaction conditions, though the reverse reaction appears to be unfeasible. Both compounds **I** and **IIa** were found to transform to two distinct Mn-oxo cluster compounds under suitable reaction conditions. Successful exchange of the lattice solvent molecules (DMA) in **I** by water molecules resulted in high proton mobility with conductivity values reaching ~0.87 × 10^{-3} Ω^{-1} cm^{-1} at 34 °C and 98% RH, which is comparable to some of the best values reported in the literature. Magnetic studies on the parent compounds indicate only antiferromagnetic behavior. Partial substitution of the Mn by Co in **II** resulted in a mixed metal MOF, $[CoMn_2(C_{14}H_8O_6S)_3(DMA)_2(EtOH)]\cdot DMA$, **III**, which on decomposition gave rise to $CoMn_2O_4$ spinel phases with particle sizes in the nanoregime. The present study suggests a new precursor source for the preparation of useful ceramic oxides.

■ ASSOCIATED CONTENT

Supporting Information

IR, UV−visible spectra of the compounds; PXRD patterns and TGA of the compounds; important bond distances, bond angles and hydrogen bond distances in the compounds and additional structural figures. This material is available free of charge via the Internet at http://pubs.acs.org.

■ AUTHOR INFORMATION

Corresponding Author

*E-mail: snatarajan@sscu.iisc.ernet.in.

Notes

The authors declare no competing financial interest.

■ ACKNOWLEDGMENTS

Authors thank the Council of Scientific and Industrial Research (CSIR), Government of India, for the award of a fellowship (S.B.) and a research grant (S.N.). S.N. thanks the Department of Science and Technology (DST), Government of India, for the award of a research grant. DST is also thanked for a J. C. Bose National Fellowship (S.N.). DST-Nano Mission is thanked for financial support (A.J.B.).

■ REFERENCES

(1) (a) Special Issue on Metal Orgainc Frameworks. *Chem. Rev.* **2012**, *112*, 673−1268 and references therein. (b) MacGillivray, L. R. *Metal Organic Frameworks: Design and Applications*; Wiley: New York, 2010. (c) Farrusseng, D. *Metal Organic Frameworks: Applications from Catalysis to Gas Storage*; Wiley-VCH: New York, 2011.

(2) (a) Jiang, H.-L.; Xu, Q. *Chem. Commun.* **2011**, *47*, 3351−3370. (b) Suh, M. P.; Park, H. J.; Prasad, T. K.; Lim, D.-W. *Chem. Rev.* **2011**, *112*, 782−835. (c) Schröder, M. *Functional Metal-Organic Frameworks: Gas Storage, Separation and Catalysis*; Springer: Berlin, 2010. (d) Murray, L. J.; Dinca, M.; Long, J. R. *Chem. Soc. Rev.* **2009**, *38*, 1294−1314. (e) Li, J.-R.; Kuppler, R. J.; Zhou, H.-C. *Chem. Soc. Rev.* **2009**, *38*, 1477−1504. (f) Burtch, N. C.; Jasuja, H.; Walton, K. S. *Chem. Rev.* **2014**, *114*, 10575−10612.

(3) (a) Liu, D.; Lu, K.; Poon, C.; Lin, W. *Inorg. Chem.* **2013**, *53*, 1916−1924. (b) Kreno, L. E.; Leong, K.; Farha, O. K.; Allendorf, M.; Van Duyne, R. P.; Hupp, J. T. *Chem. Rev.* **2011**, *112*, 1105−1125. (c) Gole, B.; Bar, A. K.; Mukherjee, P. S. *Chem. Commun.* **2011**, *47*, 12137−12139. (d) Gole, B.; Bar, A. K.; Mukherjee, P. S. *Chem.—Eur. J.* **2014**, *20*, 2276−2291.

(4) (a) Yoon, M.; Srirambalaji, R.; Kim, K. *Chem. Rev.* **2011**, *112*, 1196−1231. (b) Uemura, T.; Yanai, N.; Kitagawa, S. *Chem. Soc. Rev.* **2009**, *38*, 1228−1236.

(5) Kurmoo, M. *Chem. Soc. Rev.* **2009**, *38*, 1353−1379.

(6) (a) Horcajada, P.; Gref, R.; Baati, T.; Allan, P. K.; Maurin, G.; Couvreur, P.; Férey, G.; Morris, R. E.; Serre, C. *Chem. Rev.* **2011**, *112*, 1232−1268. (b) Horcajada, P.; Serre, C.; Maurin, G.; Ramsahye, N. A.; Balas, F.; Vallet-Regí, M.; Sebban, M.; Taulelle, F.; Férey, G. *J. Am. Chem. Soc.* **2008**, *130*, 6774−6780.

(7) Kim, M.; Cahill, J. F.; Fei, H.; Prather, K. A.; Cohen, S. M. *J. Am. Chem. Soc.* **2012**, *134*, 18082−18088.

(8) (a) Yoon, M.; Suh, K.; Natarajan, S.; Kim, K. *Angew. Chem., Int. Ed.* **2013**, *52*, 2688−2700. (b) Ramaswamy, P.; Wong, N. E.; Shimizu, G. K. H. *Chem. Soc. Rev.* **2014**, *43*, 5913−5932.

(9) (a) Gür, T. M. *Chem. Rev.* **2013**, *113*, 6179−6206. (b) Ormerod, R. M. *Chem. Soc. Rev.* **2003**, *32*, 17−28. (c) Wang, Y.-J.; Qiao, J.; Baker, R.; Zhang, J. *Chem. Soc. Rev.* **2013**, *42*, 5768−5787. (d) Zhang, H.; Shen, P. K. *Chem. Rev.* **2012**, *112*, 2780−2832. (e) Zhang, H.; Shen, P. K. *Chem. Soc. Rev.* **2012**, *41*, 2382−2394. (f) Service, R. F. *Science* **2002**, *296*, 1222−1224. (g) Kreuer, K.-D.; Paddison, S. J.; Spohr, E.; Schuster, M. *Chem. Rev.* **2004**, *104*, 4637−4678. (h) Peighambardoust, S. J.; Rowshanzamir, S.; Amjadi, M. *Int. J. Hydrogen Energy* **2010**, *35*, 9349−9384. (i) Yoon, M.; Suh, K.; Kim, H.; Kim, Y.; Selvapalam, N.; Kim, K. *Angew. Chem.* **2011**, *123*, 8016−8019. (j) Laberty-Robert, C.; Valle, K.; Pereira, F.; Sanchez, C. *Chem. Soc. Rev.* **2011**, *40*, 961−1005. (k) Tolle, P.; Kohler, C.; Marschall, R.; Sharifi, M.; Wark, M.; Frauenheim, T. *Chem. Soc. Rev.* **2012**, *41*, 5143−5159. (l) McKeen, J. C.; Yan, Y. S.; Davis, M. E. *Chem. Mater.* **2008**, *20*, 3791−3793. (m) Basak, D.; Versek, C.; Toscano, D. T.; Christensen, S.; Tuominen, M. T.; Venkataraman, D. *Chem. Commun.* **2012**, *48*, 5922−5924.

(10) (a) Yamada, T.; Otsubo, K.; Makiura, R.; Kitagawa, H. *Chem. Soc. Rev.* **2013**, *42*, 6655−6669. (b) Li, S.-L.; Xu, Q. *Energy Environ. Sci.* **2013**, *6*, 1656−1683.

(11) (a) Nagarkar, S. S.; Unni, S. M.; Sharma, A.; Kurungot, S.; Ghosh, S. K. *Angew. Chem., Int. Ed.* **2014**, *53*, 2638−2642. (b) Kim, S.; Dawson, K. W.; Gelfand, B. S.; Taylor, J. M.; Shimizu, G. K. H. *J. Am. Chem. Soc.* **2013**, *135*, 963−966. (c) Shimizu, G. K. H.; Taylor, J. M.; Kim, S. *Science* **2013**, *341*, 354−355. (d) Sadakiyo, M.; Yamada, T.; Kitagawa, H. *J. Am. Chem. Soc.* **2009**, *131*, 9906−9907. (e) Bazaga-García, M.; Colodrero, R. M. P.; Papadaki, M.; Garczarek, P.; Zoń, J.; Olivera-Pastor, P.; Losilla, E. R.; León-Reina, L.; Aranda, M. A. G.; Choquesillo-Lazarte, D.; Demadis, K. D.; Cabeza, A. *J. Am. Chem. Soc.* 2014. (f) Panda, T.; Kundu, T.; Banerjee, R. *Chem. Commun.* **2012**, *48*, 5464−5466. (g) Sen, S.; Nair, N. N.; Yamada, T.; Kitagawa, H.; Bharadwaj, P. K. *J. Am. Chem. Soc.* **2012**, *134*, 19432−19437. (h) Pardo, E.; Train, C.; Gontard, G.; Boubekeur, K.; Fabelo, O.; Liu, H.; Dkhil, B.; Lloret, F.; Nakagawa, K.; Tokoro, H.; Ohkoshi, S.-i.; Verdaguer, M. *J. Am. Chem. Soc.* **2011**, *133*, 15328−15331. (i) Yamada, T.; Sadakiyo, M.; Kitagawa, H. *J. Am. Chem. Soc.* **2009**, *131*, 3144−3145. (j) Zhao, X.; Mao, C.; Bu, X.; Feng, P. *Chem. Mater.* **2014**, *26*, 2492−2495. (k) Ramaswamy, P.; Matsuda, R.; Kosaka, W.; Akiyama, G.; Jeon, H. J.; Kitagawa, S. *Chem. Commun.* **2014**, *50*, 1144−1146. (l) Bhattacharya, S.; Gnanavel, M.; Bhattacharyya, A. J.; Natarajan, S. *Cryst. Growth Des.* **2013**, *14*, 310−325. (m) Sahoo, S. C.; Kundu, T.; Banerjee, R. *J. Am. Chem. Soc.* **2011**, *133*, 17950−17958. (n) Taylor, J. M.; Mah, R. K.; Moudrakovski, I. L.; Ratcliffe, C. I.; Vaidhyanathan, R.; Shimizu, G. K. H. *J. Am. Chem. Soc.* **2010**, *132*, 14055−14057. (o) Jeong, N. C.; Samanta, B.; Lee, C. Y.; Farha, O. K.; Hupp, J. T. *J. Am. Chem. Soc.* **2011**, *134*, 51−54.

(12) (a) Tanabe, K. K.; Cohen, S. M. *Chem. Soc. Rev.* **2011**, *40*, 498−519. (b) Horike, S.; Shimomura, S.; Kitagawa, S. *Nat. Chem.* **2009**, *1*, 695−704.

(13) (a) Kawano, M.; Fujita, M. *Coord. Chem. Rev.* **2007**, *251*, 2592−2605. (b) Liu, D.; Lang, J.-P.; Abrahams, B. F. *J. Am. Chem. Soc.* **2011**, *133*, 11042−11045. (c) Reger, D. L.; Debreczeni, A.; Smith, M. D. *Inorg. Chem.* **2011**, *50*, 11754−11764. (d) Chen, M.-S.; Chen, M.; Takamizawa, S.; Okamura, T.-a.; Fan, J.; Sun, W.-Y. *Chem. Commun.* **2011**, *47*, 3787−3789. (e) Su, Z.; Chen, M.; Okamura, T.-a.; Chen,

DOI: 10.1021/ic5018517
Inorg. Chem. 2015, 54, 1254−1271

M.-S.; Chen, S.-S.; Sun, W.-Y. *Inorg. Chem.* **2011**, *50*, 985−991. (f) Inokuma, Y.; Arai, T.; Fujita, M. *Nat. Chem.* **2010**, *2*, 780−783. (g) Ghosh, S. K.; Zhang, J.-P.; Kitagawa, S. *Angew. Chem., Int. Ed.* **2007**, *46*, 7965−7968. (h) MacGillivray, L. R.; Papaefstathiou, G. S.; Friščić, T.; Hamilton, T. D.; Bučar, D.-K.; Chu, Q.; Varshney, D. B.; Georgiev, I. G. *Acc. Chem. Res.* **2008**, *41*, 280−291. (i) Liu, D.; Ren, Z.-G.; Li, H.-X.; Lang, J.-P.; Li, N.-Y.; Abrahams, B. F. *Angew. Chem., Int. Ed.* **2010**, *49*, 4767−4770. (j) Gadzikwa, T.; Farha, O. K.; Mulfort, K. L.; Hupp, J. T.; Nguyen, S. T. *Chem. Commun.* **2009**, 3720−3722. (k) Costa, J. S.; Gamez, P.; Black, C. A.; Roubeau, O.; Teat, S. J.; Reedijk, J. *Eur. J. Inorg. Chem.* **2008**, *2008*, 1551−1554.

(14) (a) Manos, M. J.; Kyprianidou, E. J.; Papaefstathiou, G. S.; Tasiopoulos, A. J. *Inorg. Chem.* **2012**, *51*, 6308−6314. (b) Das, M. C.; Bharadwaj, P. K. *J. Am. Chem. Soc.* **2009**, *131*, 10942−10949. (c) Neogi, S.; Sen, S.; Bharadwaj, P. K. *CrystEngComm* **2013**, *15*, 9239−9248. (d) Sarma, D.; Ramanujachary, K. V.; Lofland, S. E.; Magdaleno, T.; Natarajan, S. *Inorg. Chem.* **2009**, *48*, 11660−11676. (e) Kyprianidou, E. J.; Lazarides, T.; Kaziannis, S.; Kosmidis, C.; Itskos, G.; Manos, M. J.; Tasiopoulos, A. J. *J. Mater. Chem. A* **2014**, *2*, 5258−5266. (f) Reger, D. L.; Horger, J. J.; Smith, M. D. *Chem. Commun.* **2011**, *47*, 2805−2807.

(15) (a) Mahata, P.; Sarma, D.; Madhu, C.; Sundaresen, A.; Natarajan, S. *Dalton Trans.* **2011**, *40*, 1952−1960. (b) Sarma, D.; Mahata, P.; Natarajan, S. *Curr. Sci.* **2012**, *103*, 1185−1192. (c) Mahata, P.; Sankar, G.; Madras, G.; Natarajan, S. *Chem. Commun.* **2005**, 5787−5789.

(16) Nakamoto, K. *Infrared and Raman Spectra of Inorganic and Coordination Compounds, Theory and Applications in Inorganic Chemistry*. Wiley: New York, 2008.

(17) Lever, A. B. P. *Inorganic Electronic Spectroscopy*; Elsevier: Amsterdam, 1984.

(18) (a) Blasse, G.; Grabmaier, B. C. *Luminescent Materials*; Springer-Verlag: Berlin, 1994. (b) Song, W.-C.; Li, J.-R.; Song, P.-C.; Tao, Y.; Yu, Q.; Tong, X.-L.; Bu, X.-H. *Inorg. Chem.* **2009**, *48*, 3792−3799.

(19) *CrysAlis CCD and CrysAlis PRO RED*, version 1.171.33.34d; Oxford Diffraction Ltd.: Abingdon, Boxfordshire, England, 2009.

(20) Sheldrick, G. M. *SHELXS-97, Program for Crystal Structure Solution and Refinement*; University of Göttingen: Göttingen, Germany, 1997.

(21) Farrugia, L. *J. Appl. Crystallogr.* **1999**, *32*, 837.

(22) van der Sluis, P.; Spek, A. L. *Acta Crystallogr., Sect. A: Found. Crystallogr.* **1990**, *46*, 194.

(23) (a) Han, L.; Zhou, Y.; Wang, X.-T.; Li, X.; Tong, M.-L. *J. Mol. Struct.* **2009**, *923*, 24−27. (b) Wang, Y.-Q.; Liu, H.-T.; Qi, Y.; Gao, E.-Q. *Dalton Trans.* **2014**, *43*, 11819−11825. (c) Zhong, R.-Q.; Zou, R.-Q.; Du, M.; Yamada, T.; Maruta, G.; Takeda, S.; Li, J.; Xu, Q. *CrystEngComm* **2010**, *12*, 677−681. (d) Chen, X.; Wang, Y.-Y.; Liu, B.; Yin, B.; Liu, P.; Shi, Q.-Z. *Dalton Trans.* **2013**, *42*, 7092−7100. (e) Wang, Y.-Q.; Yue, Q.; Qi, Y.; Wang, K.; Sun, Q.; Gao, E.-Q. *Inorg. Chem.* **2013**, *52*, 4259−4268. (f) Zhao, J.-P.; Hu, B.-W.; Yang, Q.; Zhang, X.-F.; Hu, T.-L.; Bu, X.-H. *Dalton Trans.* **2010**, *39*, 56−58. (g) Wang, X.; Liu, L.; Conato, M.; Jacobson, A. J. *Cryst. Growth Des.* **2011**, *11*, 2257−2263.

(24) (a) Ma, L.-F.; Han, M.-L.; Qin, J.-H.; Wang, L.-Y.; Du, M. *Inorg. Chem.* **2012**, *51*, 9431−9442. (b) Li, X.; Li, J.; Li, M.-K.; Fei, Z. *Z. Anorg. Allg. Chem.* **2014**, *640*, 1479−1483. (c) Agarwal, R. A.; Aijaz, A.; Ahmad, M.; Sañudo, E. C.; Xu, Q.; Bharadwaj, P. K. *Cryst. Growth Des.* **2012**, *12*, 2999−3005. (d) Chen, H.-J.; Mao, Z.-W.; Gao, S.; Chen, X.-M. *Chem. Commun.* **2001**, 2320−2321. (e) Yi, F.-Y.; Sun, Z.-M. *Cryst. Growth Des.* **2012**, *12*, 5693−5700. (f) Bauer, C. A.; Jones, S. C.; Kinnibrugh, T. L.; Tongwa, P.; Farrell, R. A.; Vakil, A.; Timofeeva, T. V.; Khrustalev, V. N.; Allendorf, M. D. *Dalton Trans.* **2014**, *43*, 2925−2935. (g) Niu, J.-J.; Li, D. *Inorg. Chem. Commun.* **2014**, *39*, 119−121. (h) He, C.-J.; Wang, W.-Y.; Wang, Y.-F. *Z. Anorg. Allg. Chem.* **2013**, *639*, 994−998. (i) Yi, F.-Y.; Dang, S.; Yang, W.; Sun, Z.-M. *CrystEngComm* **2013**, *15*, 8320−8329.

(25) (a) Alexandrov, E. V.; Blatov, V. A.; Kochetkov, A. V.; Proserpio, D. M. *CrystEngComm* **2011**, *13*, 3947−3958. (b) Blatov, V. A.; O'Keeffe, M.; Proserpio, D. M. *CrystEngComm* **2010**, *12*, 44−48.

(26) Rao, C. N. R.; Rao, K. J. *Phase Transitions in Solids: an Approach to the Study of the Chemistry and Physics of Solids*; McGraw-Hill: New York, 1978.

(27) (a) Clapham, S. E.; Hadzovic, A.; Morris, R. H. *Coord. Chem. Rev.* **2004**, *248*, 2201−2237. (b) Osborn, J. A.; Jardine, F. H.; Young, J. F.; Wilkinson, G. *Journal of the Chemical Society A: Inorganic, Physical, Theoretical* **1966**, 1711−1732. (c) Park, Y. J.; Park, J.-W.; Jun, C.-H. *Acc. Chem. Res.* **2008**, *41*, 222−234. (d) Huang, Z.; White, P. S.; Brookhart, M. *Nature* **2010**, *465*, 598−601. (e) Frech, C. M.; Blacque, O.; Schmalle, H. W.; Berke, H. *Dalton Trans.* **2006**, 4590−4598. (f) Bezzu, C. G.; Helliwell, M.; Warren, J. E.; Allan, D. R.; McKeown, N. B. *Science* **2010**, *327*, 1627−1630. (g) Warren, M. R.; Brayshaw, S. K.; Johnson, A. L.; Schiffers, S.; Raithby, P. R.; Easun, T. L.; George, M. W.; Warren, J. E.; Teat, S. J. *Angew. Chem., Int. Ed.* **2009**, *48*, 5711−5714. (h) Frech, C. M. *ChemCatChem.* **2010**, *2*, 1387−1389. (i) Crabtree, R. H. *The Organometallic Chemistry of the Transition Metals*. Wiley: New York, 2005.

(28) (a) Hu, C.; Englert, U. *Angew. Chem., Int. Ed.* **2005**, *44*, 2281−2283. (b) Mahmoudi, G.; Morsali, A. *Cryst. Growth Des.* **2007**, *8*, 391−394. (c) Zhang, Y.-J.; Liu, T.; Kanegawa, S.; Sato, O. *J. Am. Chem. Soc.* **2009**, *131*, 7942−7943. (d) Song, Y.-m.; Luo, F.; Luo, M.-b.; Liao, Z.-w.; Sun, G.-m.; Tian, X.-z.; Zhu, Y.; Yuan, Z.-J.; Liu, S.-j.; Xu, W.-y.; Feng, X.-f. *Chem. Commun.* **2012**, *48*, 1006−1008.

(29) (a) Hutchins, K. M.; Rupasinghe, T. P.; Ditzler, L. R.; Swenson, D. C.; Sander, J. R. G.; Baltrusaitis, J.; Tivanski, A. V.; MacGillivray, L. R. *J. Am. Chem. Soc.* **2014**, *136*, 6778−6781. (b) Medishetty, R.; Husain, A.; Bai, Z.; Runčevski, T.; Dinnebier, R. E.; Naumov, P.; Vittal, J. J. *Angew. Chem., Int. Ed.* **2014**, *53*, 5907−5911. (c) Medishetty, R.; Koh, L. L.; Kole, G. K.; Vittal, J. J. *Angew. Chem., Int. Ed.* **2011**, *50*, 10949−10952.

(30) (a) Kim, Y.; Das, S.; Bhattacharya, S.; Hong, S.; Kim, M. G.; Yoon, M.; Natarajan, S.; Kim, K. *Chem.—Eur. J.* **2012**, *18*, 16642−16648. (b) Das, S.; Kim, H.; Kim, K. *J. Am. Chem. Soc.* **2009**, *131*, 3814−3815. (c) Song, X.; Jeong, S.; Kim, D.; Lah, M. S. *CrystEngComm* **2012**, *14*, 5753−5756. (d) Song, X.; Kim, T. K.; Kim, H.; Kim, D.; Jeong, S.; Moon, H. R.; Lah, M. S. *Chem. Mater.* **2012**, *24*, 3065−3073. (e) Shultz, A. M.; Sarjeant, A. A.; Farha, O. K.; Hupp, J. T.; Nguyen, S. T. *J. Am. Chem. Soc.* **2011**, *133*, 13252−13255. (f) Liu, T.-F.; Zou, L.; Feng, D.; Chen, Y.-P.; Fordham, S.; Wang, X.; Liu, Y.; Zhou, H.-C. *J. Am. Chem. Soc.* **2014**, *136*, 7813−7816. (g) Dinca, M.; Long, J. R. *J. Am. Chem. Soc.* **2007**, *129*, 11172−11176.

(31) (a) Jeong, S.; Kim, D.; Song, X.; Choi, M.; Park, N.; Lah, M. S. *Chem. Mater.* **2013**, *25*, 1047−1054. (b) Li, T.; Kozlowski, M. T.; Doud, E. A.; Blakely, M. N.; Rosi, N. L. *J. Am. Chem. Soc.* **2013**, *135*, 11688−11691. (c) Burnett, B. J.; Barron, P. M.; Hu, C.; Choe, W. *J. Am. Chem. Soc.* **2011**, *133*, 9984−9987.

(32) (a) Das, R. K.; Aijaz, A.; Sharma, M. K.; Lama, P.; Bharadwaj, P. K. *Chem.—Eur. J.* **2012**, *18*, 6866−6872. (b) Ikemoto, K.; Inokuma, Y.; Fujita, M. *J. Am. Chem. Soc.* **2011**, *133*, 16806−16808.

(33) (a) Liu, Q.-K.; Ma, J.-P.; Dong, Y.-B. *J. Am. Chem. Soc.* **2010**, *132*, 7005−7017. (b) Li, X.; Xu, H.; Kong, F.; Wang, R. *Angew. Chem., Int. Ed.* **2013**, *52*, 13769−13773.

(34) (a) Addison, A. W.; Rao, T. N.; Reedijk, J.; van Rijn, J.; Verschoor, G. C. *J. Chem. Soc., Dalton Trans.* **1984**, 1349−1356. (b) Bhattacharya, S.; Sanyal, U.; Natarajan, S. *Cryst. Growth Des.* **2011**, *11*, 735−747.

(35) Liang, X.; Zhang, F.; Feng, W.; Zou, X.; Zhao, C.; Na, H.; Liu, C.; Sun, F.; Zhu, G. *Chem. Sci.* **2013**, *4*, 983−992.

(36) (a) Goodenough, J. B. *Magnetism and the Chemical Bond*; Interscience Publishers: Olney, Bucks, U.K., 1963. (b) Mahata, P.; Sarma, D.; Natarajan, S. *J. Chem. Sci.* **2010**, *122*, 19−35. (c) Rodríguez-Fortea, A.; Alemany, P.; Alvarez, S.; Ruiz, E. *Chem.—Eur. J.* **2001**, *7*, 627−637.

(37) Scherrer, P. *Nachr. Ges. Wiss. Göttingen Math.-Phys. Klasse* **1918**, *26*, 98.

(38) Cheng, R.; Shu, Y.; Li, L.; Zheng, M.; Wang, X.; Wang, A.; Zhang, T. *Appl. Catal., A* **2007**, *316*, 160−168.

(39) (a) Gubi, S. P. *Magnetic Nanoparticles*; Wiley: New York, 2009. (b) Nealon, G. L.; Donnio, B.; Greget, R.; Kappler, J.-P.; Terazzi, E.;

DOI: 10.1021/ic5018517
Inorg. Chem. 2015, 54, 1254−1271

Gallani, J. L. *Nanoscale* **2012**, *4*, 5244. (c) Kolhatkar, A. G.; Jamison, A. C.; Litvinov, D.; Willson, R. C.; Lee, T. R. *Int. J. Mol. Sci.* **2013**, *14*, 15977−16009. (d) Fang, M.; Ström, V.; Olsson, R. T.; Belova, L.; Rao, K. V. *Nanotechnology* **2012**, *23*, 145601. (e) Boucher, B.; Buhl, R.; Perrin, M. *J. Appl. Phys.* **1968**, *39*, 632−634.
(40) (a) Wickham, D. G.; Croft, W. J. *J. Phys. Chem. Solids* **1958**, *7*, 351−360. (b) Bordeneuve, H.; Tenailleau, C.; Guillemet-Fritsch, S.; Smith, R.; Suard, E.; Rousset, A. *Solid State Sci.* **2010**, *12*, 379−386.

DOI: 10.1021/ic5018517
Inorg. Chem. 2015, 54, 1254−1271